The Journal of Undergraduate Research in Physics

APPARATUS FOR MEASURING DOUBLE DIFFERENTIAL CROSS SECTIONS FOR ELECTRON EMISSION IN ION-ATOM COLLISIONS 2
Mark Behrens
Kansas State University

A STUDY OF THE VACCINE EFFECT IN TRIGLYCINE SULFATE USING POLARIZATION SWITCHING MEASUREMENTS 7
Joseph J. Vandiver
California State University San Bernardino

STABLE FREQUENCIES OF A VERTICAL ROTATING CHAIN 11
Jordana L. Lacy
Juniata College

NEUTRON SCATTERING: Magnetic Flux Tube 15
Andrei Teodor Filip and Dan Adrian Mazilu
Alexandru Ioan Cuza University

DIFFUSION OF SOLAR ENERGETIC PARTICLES: A Numerical Study 20
Kenneth B. Baile
Roanoke College

ADIABATIC POPULATION TRANSFER IN A THREE LEVEL ATOM 25
James V. Ruffo
University of Rochester

POST USE BOOK REVIEW 30
COLLEGE PHYSICS, 4th Ed. R.A. Serway and J.S. Faughn
PHYSICS, 3rd Ed. J.D. Cutnell and K.W. Johnson
Hilary Davis
Guilford College

On preparing a manuscript for publication in JURP 31

Volume 15, Number 1
Winter, 1996

Produced by the Physics Department of Guilford College
for
The American Institute of Physics and the Society of Physics Students

THE JOURNAL OF UNDERGRADUATE RESEARCH IN PHYSICS

This journal is devoted to research work done by undergraduate students in physics and its related fields. It is to be a vehicle for the exchange of ideas and information by undergraduate students. Information for students wishing to submit manuscripts for possible inclusion in the Journal follows.

ELIGIBILITY
The author(s) must have performed all work reported in the paper as an undergraduate student(s). The subject matter of the paper is open to any area of pure or applied physics or physics related field.

SPONSORSHIP
Each paper must be sponsored by a full-time faculty member of the department in which the research was done. A letter from the sponsor, certifying that the work was done by the author as an undergraduate and that the sponsor is willing to be acknowledged at the end of the paper, must accompany the manuscript if it is to be considered for publication.

SUBMISSION
Two copies of the manuscript, the letter from the sponsor and a telephone number or E-Mail address where the author can be reached should be sent to:

Dr. Rexford E. Adelberger, Editor
THE JOURNAL OF UNDERGRADUATE
RESEARCH IN PHYSICS
Physics Department
Guilford College
Greensboro, NC 27410

FORM
The manuscript should be typed, double spaced, on 8 1/2 x 11 inch sheets. Margins of about 1.5 inches should be left on the top, sides, and bottom of each page. Papers should be limited to fifteen pages of text in addition to an abstract (not to exceed 250 words) and appropriate drawings, pictures, and tables.

Manuscripts may be submitted on a disk that can be read by a MacIntosh™. The files must be compatible with MacWrite™, MicroSoft Word™ , PageMaker™ or WordPerfect™.

ILLUSTRATIONS
Line drawings should be made with black ink on plain white paper. Each figure or table must be on a separate sheet. Photographs must have a high gloss finish. If the submission is on a disk, the illustrations should be in PICT, TIFF or EPS format.

CAPTIONS
A brief caption should be provided for each illustration or table, but it should not be part of the figure. The captions should be listed together at the end of the manuscript

EQUATIONS
Equations should appear on separate lines, and may be written in black ink. We use EXPRESSIONIST™ to format equations in the Journal.

FOOTNOTES
Footnotes should be typed, double spaced and grouped together in sequence at the end of the manuscript.

PREPARING A MANUSCRIPT
A more detailed set of instructions for authors wishing to prepare manuscripts for publication in the Journal of Undergraduate Research in Physics can be found in the back of each issue.

SUBSCRIPTION INFORMATION

The Journal is published twice each academic year, issue # 1 appearing in November and issue # 2 in May of the next year. There are two issues per volume.

TYPE OF SUBSCRIBER	PRICE PER VOLUME
Individual	$US 5.00
Institution	$US 10.00

Foreign subscribers add $US 2.00 for surface postage, $US 10.00 for air freight.

Back issues may be purchased by sending $US 15.00 per volume to the editorial office.

To receive a subscription, send your name, address, and check made out to **The Journal of Undergraduate Research in Physics (JURP)** to the editorial office:

JURP
Physics Department
Guilford College
Greensboro, NC 27410

The Journal of Undergraduate Research in Physics is sent to each member of the Society of Physics Students as part of their annual dues.

VOLUME 15

ACADEMIC YEAR 1996-1997

The Journal of Undergraduate Research in Physics

ISSN 0731 - 3764

Produced by the Physics Department
of Guilford College
for
The American Institute of Physics
and
The Society of Physics Students

APPARATUS FOR MEASURING DOUBLE DIFFERENTIAL CROSS SECTIONS FOR ELECTRON EMISSION IN ION-ATOM COLLISIONS

Mark Behrens *
Department of Physics
Kansas State University
Manhattan, KS 66506-2604
received May 20, 1996

ABSTRACT

A beam of C6+ ions was accelerated to 30 MeV and directed onto a stationary molecular hydrogen gas target. The resulting ionization process was observed with a rotatable electron spectrometer, allowing for doubly differential ionization cross sections to be determined as a function of the angle and energy of the ejected electrons. This paper reports on the initial set up, testing and modification of the scattering chamber and the electron energy analyzer.

INTRODUCTION

The ionization of atomic hydrogen by fast ions cannot be described theoretically without some manner of approximation because it is a three body problem. It is analytically unsolvable both quantum mechanically and classically. Therefore, experimental investigation is necessary to fully explore the process.

An ionization cross section of an atom or molecule is proportional to the probability of ionization occurring when a certain projectile is interacts with it. A doubly differential ionization cross section (schematically shown in Figure 1) is proportional to the probability of an ionization reaction that results in an electron being ejected at an angle θ within a solid angle $d\Omega$ with an energy within the energy interval E and $E + dE$). Both the angular and energy distributions of ejected electrons are examined, hence the name doubly differential ionization cross sections (DDCS). The electron distribution produced by the ionization is axially symmetric, so only the polar angle θ is of interest. The energy spectra taken at two distinct azimuthal angles should be identical. The DDCS is obtained from the electron yield, y, and other experimentally measurable quantities through the expression:

$$DDCS \Rightarrow \frac{d^2\sigma}{d\Omega\, dE} = \frac{y}{n_i\, n_t\, \varepsilon\, \Delta\Omega\, \Delta E} \qquad (1)$$

where n_i is the number of incident projectiles, n_t is the number of targets/cm^2, $\Delta\Omega$ is the solid angle acceptance of the spectrometer and ΔE is the energy interval, and ε is the spectrometer and channeltron efficiency.

A research group at the University of Nebraska successfully measured DDCS of the ionization of molecular and atomic hydrogen at 20 to 114 keV protons. [1] Their results showed poor agreement with the plane wave Born approximation, but reasonably good agreement with continuum distorted wave approximation.

The collision chamber and experimental apparatus were then transferred to the J.R. Macdonald Laboratory at Kansas State University. This facility has a variety of accelerator equipment dedicated to atomic physics

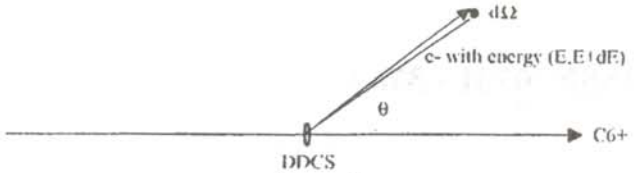

Figure 1

Schematic diagram of the scattering process. The doubly differential cross section (DDCS) is a function of the electron ejected by the interaction as well as the angle at which the electron is ejected.

Mark is a senior majoring in physics and mathematics at the University of Alabama. He participated in this NSF sponsored research experience during the summer prior to his junior year. Originally from Milwaukee, Wisconsin, he spent most of his pre-collegiate life assuming that he would become a professional musician. Music still remains a welcome retreat. He is presently applying to graduate schools in pursuit of a Ph.D. program in pure mathematics, a field in which has always harbored a keen interest.

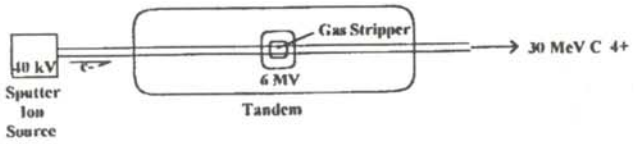

Figure 2
Schematic diagram of the tandem accelerator. Ions from the sputter source are initially accelerated by the high voltage platform and then by the tandem Van de Graaff. The gas stripper in the center of the high voltage terminal strips the ions of all but two electrons.

research, including a 7.5 MV tandem Van de Graaf accelerator and a superconducting linear accelerator (LINAC). This meant that the Nebraska experiment could be extended to higher energies and heavier ions. The initial attempt at using this apparatus in 1994 resulted in electron energy spectra that defied theoretical expectations in the low energy region. While it was possible that these data were genuine, a fault in the apparatus was deemed to be the culprit.

EXPERIMENTAL SETUP AND APPARATUS

The tandem Van de Graaff accelerator was used to accelerate C^{+6} ions to 30 MeV. The C^{+6} ions were obtained from a sputter source that sat upon a 40 kV platform (see Figure 2) A carbon cathode was bombarded with cesium, leaving the carbon atoms with an extra electron. The C^- atoms are then accelerated via the high voltage platform, focused and injected into the tandem accelerator. The C^- ions were accelerated towards the central terminal that was kept at 6 MV. A gas filled chamber, located at the terminal, stripped the carbon ions of all but 2 electrons. The C^{+4} ions were then accelerated by the terminal, resulting in an additional 24 MeV of kinetic energy. The beam was directed through a post stripping foil, removing the remaining 2 electrons from the carbon atoms. The C^{+6} was then injected into the collision chamber.

The collision chamber, shown in Figure 3, was constructed out of stainless steel, with a μmetal lining to suppress the earth's magnetic field. The chamber was evacuated to about 1 μTorr. An electrostatic energy analyzer lay on a rotatable disk within the chamber to energy analyze the scattered electrons. A Faraday cup at the end of the chamber counted the number of projectiles incident on the target. The Faraday cup is quite simple, consisting of a copper cup in the path of the beam. A copper ring was mounted just above the rim of the cup. A small negative voltage was applied between the ring and the cup to prevent the escape of secondary electrons produced when the beam particles hit the copper cup. By reading the current flowing from the cup to ground, the beam flux could be determined.

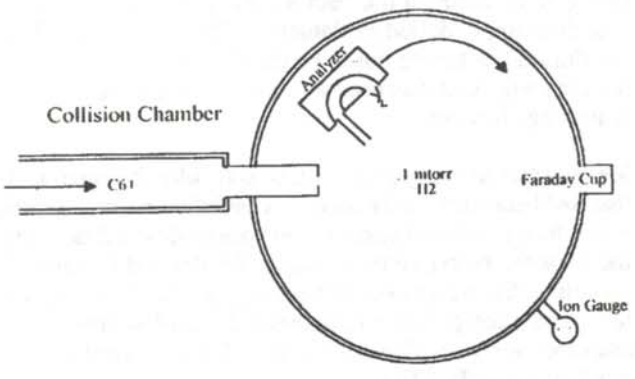

Figure 3
Schematic diagram of the collision chamber. The electron spectrometer rotates about the interaction region to measure the angular dependence of the DDCS.

A hemispherical electrostatic electron energy analyzer, shown in Figure 4, was used to detect the secondary electrons. The electrodes and housing were constructed of copper to discourage local magnetization. The surfaces of the hemispheres were coated with soot to reduce electron emission due to collisions of electrons with the surfaces. Electrodes at the entrance and exits of the analyzer gave the option of accelerating or decelerating the electrons before they passed through the analyzer. If the voltages $Vcom1 = Vcom2 = Vcom$ (see Figure 4), an electron of kinetic energy T will successfully traverse the analyzer and be detected by the channeltron if the hemispheres have voltages HV_1 and HV_2 given by:

$$HV_1 = \left[\frac{T + e\,(Vcom)}{e}\right]\frac{r_2 - r_1}{r_1}$$
$$HV_1 = -\left[\frac{T + e\,(Vcom)}{e}\right]\frac{r_2 - r_1}{r_2}, \qquad (2)$$

where r_1 and r_2 are the radii of the inner and outer hemispheres respectively and e is the charge on the electron.

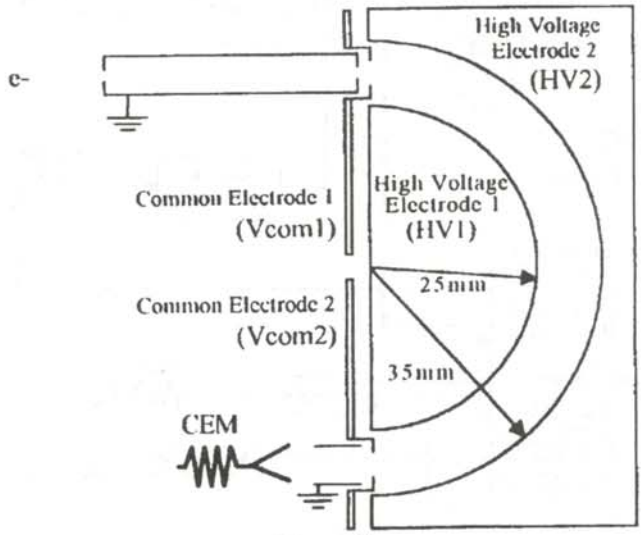

Figure 4
Schematic diagram of the electron spectrometer. Note that the analyzer's symmetry is spherical, not cylindrical.

A channeltron, or CEM, is a semiconductor electron detector that operates in a fashion similar to a photomultiplier tube. It consists of a small cone with a coil of tubing leading out of the rear, all of which is coated with a semiconducting material on the interior. The cone is biased with a small positive voltage, while a large positive voltage is applied to the rear. An incident electron displaces a few electrons from the semiconducting surface. These in turn displace more electrons, initiating an electron avalanche of sufficient strength to produce a measurable signal.

The whole system was controlled by a microVAX computer as shown in Figure 5. A large amount of noise was picked up in the BNC cables going in and out of the preamp, so it was necessary to wrap the entire preamp, as well as the cable in aluminum foil and make sure that there was only 1 ground. The remaining small amount of noise was eliminated by setting the discriminator threshold at an appropriate level.

A modified data acquisition program was developed. The system communicates with the apparatus via a FORTRAN/VMS environment called XSYS, an event driven language. A menu driven interface, written in FORTRAN, was designed. The original program was modified to display the status of the run as it progressed and new options introduced to allow for a more accurate stepping of the voltages on the electron analyzer. The modified program displayed two graphs: one which gave the raw count rate; one that divided the raw count rate by the energy to account for dispersion. The data was stored on an 80MB disk pack for future analysis.

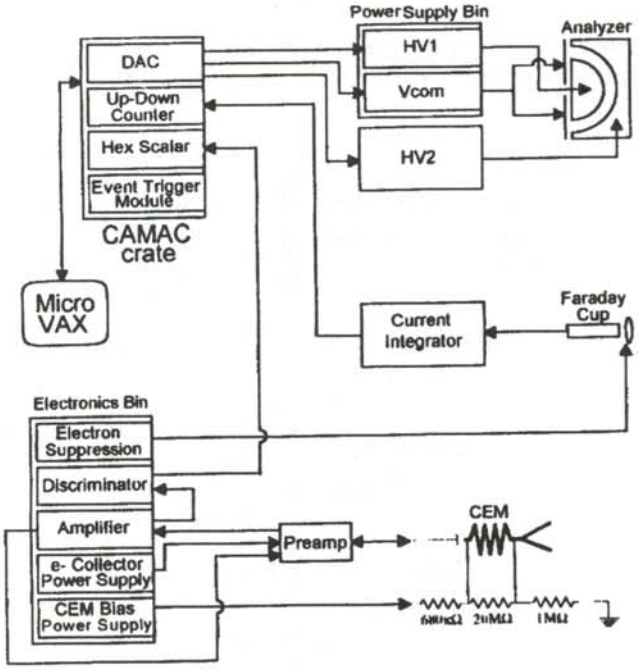

Figure 5
Schematic diagram of the electronics used to control the experiment.

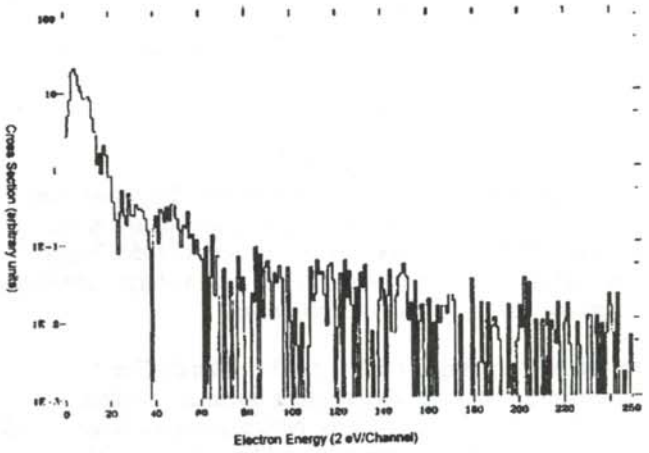

Figure 6
Cross section vs electron energy at 140 degrees. This is one of the first spectra we took. These results were not what we expected.

RESULTS

Carrying out the experiment was, in fact, much more difficult then it seemed it should at the first glance. Initially, the challenge was in understanding the apparatus. While the equipment had been used by many different people, none of the presently involved individuals had much experience with it. The software had to be understood and modified, and the electronic systems tested.

The first problem we found was a collimation misalignment which prevented most of the ion beam from traversing the interaction region. When one of the collimators was removed and the collimation left to a 2 mm hole directly before the interaction region and a series of 4 jaw slits before the beam line. This produced a improvement in beam transmission. We were now able to get as much as 40 nA of ion current in the chamber Faraday cup. The electron spectra, however, were very puzzling. Many showed little more than background, while some backward angle data exhibited the expected low energy beak (as seen in Figure 6), many of our backward angle spectra showed data that simply defied explanation. The cause of much of our difficulties turned out to be the electrons produced by the ion gauge that was used to measure the pressure in the scattering chamber.

We entertained many possibilities as to why the apparatus that had been previously used successfully was now failing to produce consistent results. One possibility had do with the preaccelerating voltage (V_{com}). We derived Equation 2 assuming that fringe effects were negligible. Using an ion lens simulation program to numerically explore this situation, we found that edge effects did not contribute much to our difficulties.

In the next run, nearly every angle seemed to present a low energy deficiency in the cross section, as shown in Figure 7. We needed to find out was causing the disappearance of

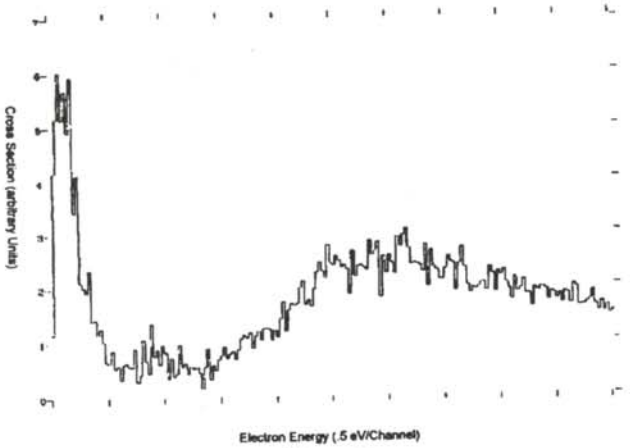

Figure 7

Cross section vs electron energy at 90 degrees. This spectrum was characteristic of the second run results.

the low energy electrons. The preaccelerating voltage (Vcom) was increased gradually from 0 to 40 V, causing a gain in the 'dip' area, but the slope of the cross section seemed to be too gradual. Even more curious was an asymmetry in the spectrum. Spectra taken at 90 degrees on one side did not agree with spectra taken at 90 degrees on the other side. This is symptomatic of slit scattering, but changing the current on the slit did not cause any significant changes. Perhaps some stray electric or magnetic field may be the culprit. The interaction region was protected by μmetal and the spectrometer was housed in a copper casing with brass screws, so a magnetic field seemed unlikely. It was suggested that oil from the roughing pump and the diffusion pump was collecting on the surfaces of the apparatus, charging up over time. The electric fields caused by such a phenomenon would be insufficient to affect high energy electrons but the low energy electrons might be deflected.

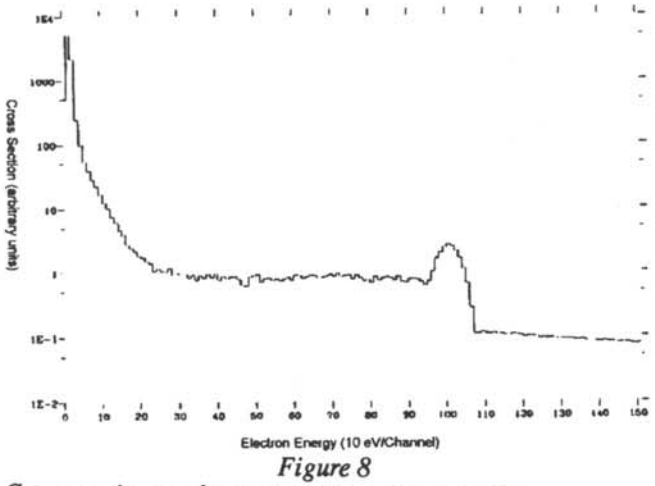

Figure 8

Cross section vs electron energy. This is the first successful spectrum where a 1 keV electron gun was used to produce the incident particles

We opened the chamber and placed a 1 keV electron gun in the chamber entrance so as to simulate the experiment exactly. Spectra were taken at 90 degrees. The first spectrum is shown in Figure 8. One can readily see the low energy peak as well as the 1 keV peak of elastically scattered electrons. As time progressed, the spectra gradually become confused. This is concurrent with the contact potential theory. If oil was indeed building up charge, the stray electric fields would gradually increase in magnitude as the ions and electrons continued to collect on the nonconducting surface.

The entire chamber was cleaned with acetone (to remove the hydrocarbon based oil from the roughing pump) and trichloroethylene (to remove the silicon based oil from the diffusion pump). The spectrometer was disassembled, cleaned and resooted. The channeltron was replaced. A Gaussmeter was used to show that the μmetal shield was working well. Finally, the diffusion pump was replaced by a turbo pump, eliminating the oil problem.

This seemed to fix the problems. Figure 9 shows a spectrum taken at 30 degrees with the modified apparatus. A low energy peak is followed by a rapid drop in the cross section as the electron energy increases. This is the signature of a working spectrometer.

ACKNOWLEDGMENTS

The author would like to extend his thanks to Dr. Patrick Richard, with whom it was truly a pleasure to work, as well as to Dr. Lokesh Tribedi, Diana Ling and Gabor Toth, for their valuable guidance and friendship. He also thanks Dr. Larry Weaver for the organization of a wonderful summer research program at KSU, and the National Science Foundation for sponsoring the Research Experience for Undergraduates (REU) program. He would like to express his appreciation to Dr. Martin Stockli for his vacuumous advice and to Dr. Laszlo Baksay, to whom he owes the existence of this paper.

This work was also supported by the Division of Chemical

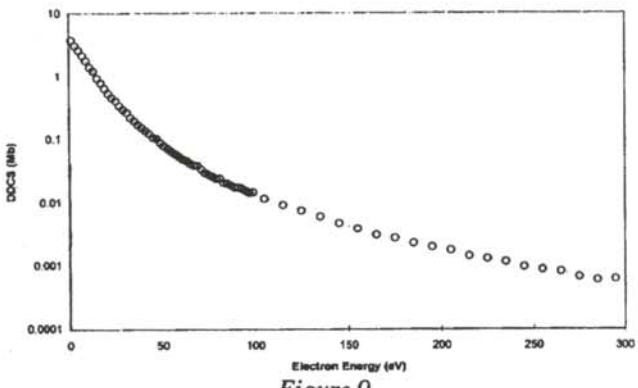

Figure 9

Cross section vs energy at 30 degrees. A spectrum taken with the modified apparatus. The error in the absolute doubly differential cross section lies between 2.2% and 4.3%.

Sciences, Office of Basic Energy Sciences, Office of Energy Research, U.S. Department of Energy.

REFERENCES

* Present address of author: Physics Department, University of Alabama, Tuscaloosa, AL MBehren1@ua1vm.ua.edu

1. G.W. Kerby III, M.W. Gealy, Y.Y. Hsu, M.E. Rudd, D.R. Schultz and C. O Reinhold, Phys. Rev. A., 51 (3), (1995), pp. 2247-2264.
2. G.W. Kerby III., *Absolute Doubly Differential Cross Sections for Ejection of Electrons in Three and Five Body Collisions of 20 to 115 keV Protons on Atomic and Molecular Hydrogen*, A Dissertation, Lincoln, Nebraska, 1994
3. Richard, et. al., private communication.

FACULTY SPONSOR

Dr. Patrick Richard
Cortelyou-Rust Distinguished Professor
Director, J.R. Macdonald Laboratory
Department of Physics
116 Cardwell Hall
Kansas State University
Manhattan, KS 66506-2604

A STUDY OF THE VACCINE EFFECT IN TRIGLYCINE SULFATE USING POLARIZATION SWITCHING MEASUREMENTS

Joseph J. Vandiver *
Department of Physics
California State University San Bernardino
San Bernardino, CA 92407-2398
received February 20, 1996

ABSTRACT

The vaccine effect was investigated using polarization switching curves. In triglycine sulfate, radiation is found to affect the hydrogen bond structure on the glycine I molecule. This causes the triglycine sulfate to loose its ferroelectric properties. The vaccine effect was reported to prevent the damage which is caused by the effect of X-radiation[1]. Several samples were prepared and polarization switching measurements were recorded for each sample. Each sample was then 'vaccinated' and irradiated. Polarization switching measurements were taken after irradiating the sample with X-rays and compared to the initial measurement. The comparison revealed a polarization loss of 26% to 86%.

1. C. Alemany, J. Mendiola, B. Jimeniz and E. Maurer, Ferroelectrics, 5, (1973), pp. 11-15

INTRODUCTION

A ferroelectric material exhibits, over some range of temperature, a spontaneous dielectric polarization which can be reversed or reoriented by application of an electric field. [1] Triglycine sulfate $(NH_2CH_2COOH)_3H_2SO_4$ (abbreviated hereafter as TGS) was discovered to have a ferroelectric nature.[2] TGS is a clear, water soluble crystal with a phase transition temperature of approximately 320K. This relatively high phase transition temperature makes TGS an excellent choice for experimental study.

Radiation, such as X-radiation, has effects on the ferroelectric properties of samples such as TGS. The radiation causes decreases of polarization, distortion of hysteresis loops, the lowering of the phase transition temperature and increasing the coercive field. The coercive field is the minimum electric field required to reverse the polarization of the sample

Joseph is currently a graduate student attending the master's program at California State University, Long Beach. This research project began in the summer of his junior year at California State University, San Bernardino, working under the supervision of Dr. Timothy Usher. In his free time, he enjoys reading, role playing games and watching movies.

The focus of this research is to attempt to verify the phenomenon known as the "vaccine effect" following a procedure similar to the one used in Reference 1 but using polarization switching curves instead of capacitance measurements. The vaccine effect occurs when the TGS sample is raised above the phase transition temperature, irradiated with X-rays for a predetermined time and then cooled to room temperature. This process has been reported to prevent the effects of radiation on the ferroelectric properties of TGS at room temperature.

Typically, a ferroelectric crystal does not have a net polarization, but is composed of many individual domains, each with a random polarization direction. A domain consists of a large number of dipoles aligned in the same direction. When an electric field is applied to a ferroelectric material, domains with directions parallel to the field will grow at the expense of the others. If the ferroelectric material is below its phase transition temperature, it will remain uniformly polarized. If an electric field of sufficient strength is applied in the antiparallel direction, the polarization of the ferroelectric dipoles will reverse orientation. This switches the polarization of the ferroelectric material.

The polarization switching curve is a plot of the current density vs time. The plot of a polarization switching curve is obtained by applying a single pulse of high voltage to the sample, generating an electric field on the order of

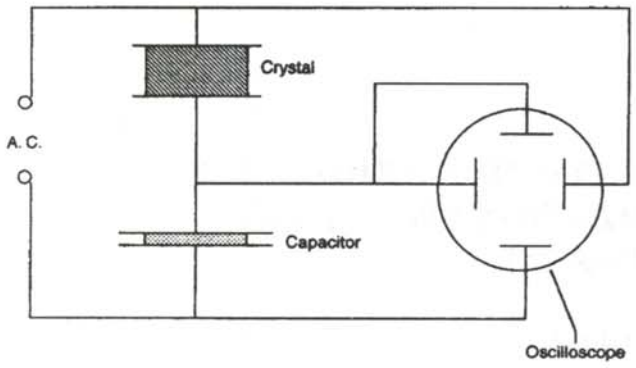

Figure 1
Schematic diagram of circuit used to determine hysteresis of the TGS sample.

1 kV/cm and measuring the current density as a function of time.. From the shape of the switching curve, we could extract a value for the polarization using the model presented in the next section.

MODEL FOR CURRENT DENSITY

A model has been developed for nucleation and growth of crystals.[4,5] This model has been refined to apply to ferroelectrics. [6] This model predicts that if the sample is suddenly hit with a sharply changing voltage, the current density, $j(t)$, through the sample as a function of time, t, will be given by:

$$j(t) = \frac{2P}{t_o}\left(\frac{t}{t_o}\right)^{n-1} \exp\left[-\left(\frac{t}{t_o}\right)^{n}\right], \qquad (1)$$

where P is the reversed polarization, t_o is a characteristic relaxation time and n is the effective dimensionality.

The effective dimensionality is related to the growth of the domain walls within the ferroelectric samples if new nucleation sites are formed during the switching process. The dimension, d, of the growth of the domain walls within the ferroelectric samples is determined in the following manner: $d = 1$ for the formation of a one dimensional domain wall; $d = 2$ for the formation of a two dimensional domain wall; $d = 3$ for a three dimensional domain growth starting from a fixed point within the sample. The dimensionality, $n = d$ if no new nucleation sites are formed during the growth of existing domains, and $n = d+1$ if new nucleation sites are formed at a constant rate during the switching process.

The exponential term in Equation 1 represents the characteristic exponential decay which commonly occurs for rate dependent processes such as radioactive decay. The remaining parts of Equation 1 represent the characteristic nucleation and growth of the domain walls within the ferroelectric samples. The data are fit to Equation 1 and a value of P extracted to determine if the vaccine effect is real.

THE EXPERIMENT

Sample Preparation

Single crystals of TGS were obtained. The crystals were cut into small slabs, ranging in thickness from 1.0 mm to 2.3 mm, cut perpendicular to the ferroelectric axis with a Lasermetric wire saw. The thickness was constant to ±0.1 mm. These small slabs were polished using undyed silk cloth wetted with distilled water. Distilled water was used because TGS is a water soluble material and would pick up minerals and chemicals found in city tap water.

The electrodes then were placed on the surface perpendicular to the ferroelectric axis. The four edges of the TGS slabs which are parallel to the ferroelectric axis were coated with a thin layer of GE 7032 varnish. The other two of the sides were affixed with wire posts. The TGS slabs were placed in a high vacuum deposition chamber where a small amount of 24K jewelers grade gold wire was placed in a tungsten boat. The bell jar of the vacuum chamber was coated with a thin layer of PAM cooking spray to prevent the gold vapor from adhering directly to the glass surface. The chamber was pumped down to approximately 2×10^{-6} Torr. A current was placed through the tungsten boat and the gold was evaporated onto the crystal surface. This procedure was repeated with the TGS samples turned over to coat the other side of the crystals. When this process was finished, the wire posts and the varnish were peeled from the edges. The sample now looks like a parallel plate capacitor.

Experimental procedure

Once the samples had been prepared, a hysteresis loop for each sample was generated using the setup shown in Figure 1. Any TGS sample with a distorted hysteresis loop was discarded because this was indicative of structural defects in the sample. Polarization switching curves where then produced using a high-voltage MOSFET bipolar square wave generator [8] as shown in Figure 2.

Several switching curves for each viable TGS sample were produced and down loaded into a computer using LAB-VIEW™ to be used as baseline data. This was the control

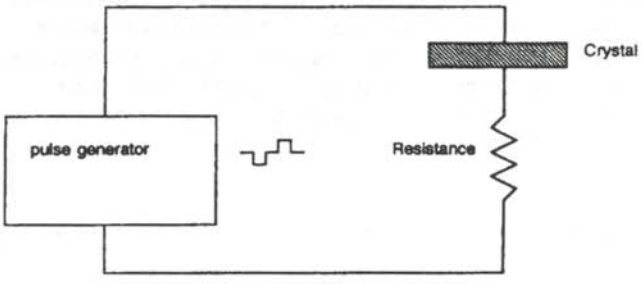

Figure 2
Schematic diagram of the circuit used to generate the switching curves for the samples. The voltage reading across the resistor, which is directly proportional to the current through the sample, was down loaded to the computer.

to show the behavior of the samples before they were radiated. The samples were then placed in a sample holder which was designed to be connected to a conventional Cu X-ray diffraction machine. The temperature of the sample was raised to 323K using a variable temperature controller. Once the target temperature had been reached, the sample was then subjected to the full spectrum of X-rays at 40 kV and 20 mA for a period of 2 hours. The sample was then cooled down to room temperature (298K) and was subjected to X-rays at the same power for an additional two hours.

The samples were then connected back to the circuit shown in Figure 2 and several more polarization switching curves were taken. An example is shown in Figure 3. The TGS polarization switching curves were fit to the current density equation and values of P, n and t_o extracted for each curve [9]. Values for the polarization, P, from the baseline date were compared to the polarization values of the X-ray treated samples.

Experimental Results and Discussion

The results which were found during the experiment are shown in Table 1. There is a wide variance in the data shown in Table 1, ranging from 26% to 86%. The data seem to suggest that the vaccination effect does not exist, but the data range is so wide spread that it not possible to say conclusively that the vaccination effect does not exist.

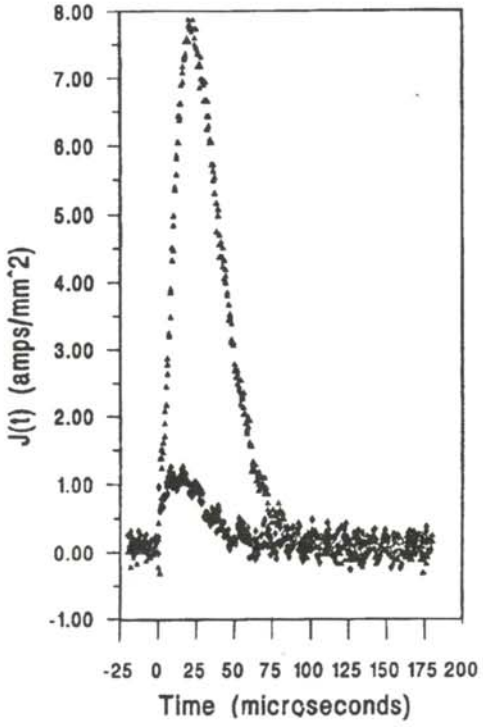

Figure 3
Polarization switching curve data for a TGS sample. This shows a comparison of the baseline data to treated data. The lower curve is the baseline data.

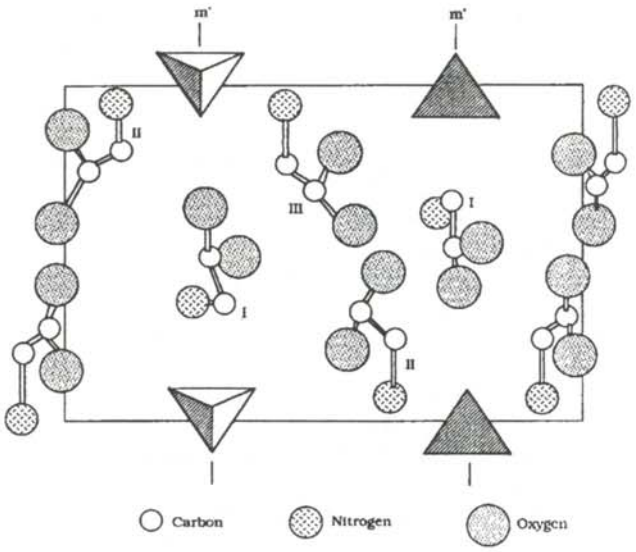

Figure 4
Diagram of the physical structure of TGS.

It has been reported [10] that irradiation brings structural changes to the hydrogen bond system in TGS. In the non-irradiated sample of TGS, the nitrogen on the glycine I molecule (see Figure 4) has three hydrogen bonds attached to it [11]. On the irradiated sample, there are only two hydrogen atoms attached to the nitrogen on the same glycine I molecule. This loss of the third hydrogen atom attached to the nitrogen on the glycine I molecule makes the polarization switching significantly more difficult due to the loss of the structural symmetry. If the "vaccine effect" exists, we think that it could somehow manage to lock in the hydrogen atoms on the clycine I molecule. It appears that this particular technique may prevent the vaccination effect from being observed.

ACKNOWLEDGMENTS

The author would like to thank Dr. Tim Usher for his advice and supervision during the course of this research. He also thanks James Channey for the development of the

Sample	P(baseline) μC/cm	P(treated) μC/cm	% difference
1	1.17	0.73	37
2	1.08	0.71	34
3	1.95	1.43	26
4	1.69	0.54	68
5	1.37	0.59	57
6	1.59	0.61	62
7	1.37	0.19	86

Table 1
Experimental results showing polarization values extracted from the switching curves.

program which allowed the data to be down loaded for processing. This research was supported by a grant from the Research Corporation (C-3119).

REFERENCES

* Current address of author: Joseph Vandiver, Department of Physics and Astronomy, California State University Long Beach, 1250 Bellflower Blvd. Long Beach, CA 90840.

1. Standard Definitions of Primary Ferroelectric Terms, ANSI/IEEE, Std. 180, (1986).
2. B.T. Matthias, C.E. Miller and J.P. Remeika, Phys. Rev., 104, (1956) p. 849.
3. C. Alemany, J. Mendiola, B. Jimeniz and E. Maurer, Ferroelectrics, 5, (1973), p. 11-15.
4. W.A. Johnson and M.F. Mehl, Trans. Am. Inst. Mining Met. Eng., 135, (1939), p. 416.
5. M. Avrami, J. Chem. Phys, 7, (1939), p. 7; M. Avrami, J. Chem. Phys., 8, (1940), p. 212; M. Avrami, J. Chem. Phys., 9, (1941), p. 177.
6. Y. Ishibashi, Jap. J. of Appl. Phys., 24, (1985), p. 126.
7. Samples were obtained from: Fast Pulse Technology, Inc. , 220 Midland Avenue, saddle Brook, NJ 07662.
8. T.D. Usher and G.A. McAuley, Rev. Sci. Instrum., 64, (1993), pp. 2027-2030.
9. We used the NLIN fitting routine developed by the SAS Institute.
10. R. Ravi and P.S. Narayanan, Ferroelectrics, 39, (1981), pp. 1221-1224.
11. E.T. Keve, Phillips Technical Review, 35, (1975).

FACULTY SPONSOR

Dr. Timothy D. Usher
Department of Physics
California State University San Bernardino
5500 University Parkway
San Bernardino, CA 92407-2397
TUsher@wiley.csusb.edu

STABLE FREQUENCIES OF A VERTICAL ROTATING CHAIN

Jordana L. Lacy *
Juniata College
Huntingdon, PA 16652
received July 30, 1996

ABSTRACT

The theory behind a vertical rotating chain predicts a close relationship with the Bessel function, $J_o(x)$. We verify Western's theory at the natural frequency. However, we found 'higher orders' of stability that are not accounted for in the original theory. Some observations are discussed.

BACKGROUND

A chain hangs vertically, attached at the upper end and free at the lower. When it is rotated about the fixed point, it is possible for the chain to form a wave with stable nodes. The positions of these nodes are similar to the zero's of the Bessel functions.

To study the nodes of the vertical rotating chain, we follow Western's model of the system [1]. Figure 1 shows the variables that will be used in the derivation. To begin, we assume small deflections and small slopes of a chain of mass density λ and length L. The assumption requires the wave on the chain to have small amplitudes. The horizontal distance from the z-axis to a point on the chain is given by r. Because the chain is fixed at one end, there is only one boundary condition:

$$\text{when } z = L, r = 0 . \tag{1}$$

The net horizontal force, F_r, acting on an mass element $\lambda\Delta z$ of the chain is given by:

$$F_r = T_h - (T_h + \Delta T_h) = -\Delta T_h = -\Delta\left[T\frac{dr}{dz}\right] , \tag{2}$$

where T_h is the horizontal component of the tension in the chain. From Figure 1, T_h can be written as:

$$T_h = T\sin(\beta) \text{ and } \tan(\beta) = \frac{dr}{dz} . \tag{3}$$

Since β is << 1, $\sin\beta \approx \tan\beta$, T_h becomes:

$$T_h = T\frac{dr}{dz} . \tag{4}$$

If the centripetal acceleration is small compared to the acceleration of gravity, then the tension, T, is approximately unaffected by the rotation:

$$T = \lambda z g . \tag{5}$$

If the amplitude of the wave on the chain is small, an element of the chain arc length, Δs, is approximately equal to Δz. Substituting Equations 2 and 5 into Newton's second law gives:

$$-\Delta\left(\lambda z g\frac{dr}{dz}\right) = \lambda\Delta z r\omega^2 , \tag{6}$$

where ω is the angular velocity of the chain element. Dividing both sides of Equation 6 by $\lambda\Delta z$, taking the limit as Δz goes to zero and expanding yields:

$$z\frac{d^2r}{dz^2} + \frac{dr}{dz} + \frac{r\omega^2}{g} = 0 . \tag{7}$$

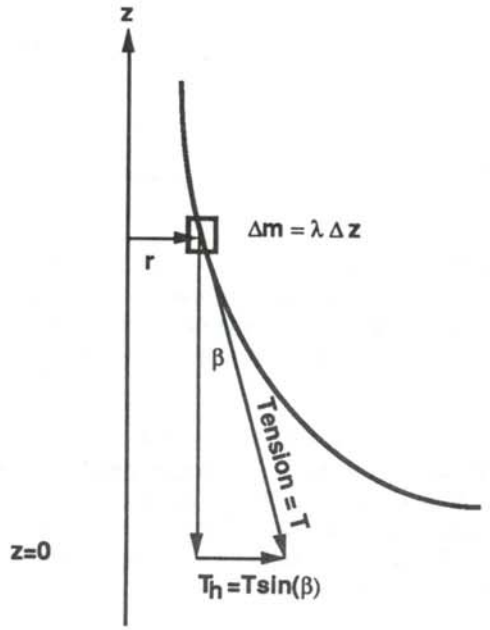

Figure 1
Schematic of the chain showing the various variables.

Jordana is a first year graduate student at the University of Delaware. This research began her junior year at Juniata College as a mini-lab project. In addition to pursuing her interests in physics, Jordana is also working towards her secondary education certificate.

To put this equation into a more familiar form, make the substitution:

$$x = 2\,\omega\sqrt{\frac{z}{g}} \tag{8}$$

into Equation 7, which gives

$$x^2\frac{d^2r}{dx^2} + x\frac{dr}{dx} + x^2 r = 0\ . \tag{9}$$

Equation 9 is Bessel's equation of zero order. The general solution to Equation 9 is:

$$r = A\,J_o(x) + B\,N_o(x)\ , \tag{10}$$

where $J_o(x)$ is a Bessel function, $N_o(x)$ is a Neumann function, and A and B are constants determined by the boundary conditions. Because we require finite solutions at both ends of the chain, $B = 0$, eliminating the $N_o(x)$ solutions [2]. Therefore, we are left with the stable, time-independent solutions of the form:

$$r = J_o\left(2\,\omega\sqrt{\frac{z}{g}}\right)\ . \tag{11}$$

Equation 11 implies that the rotating chain should have nodes (when $r = 0$) where the Bessel function $J_o(x)$ has zero's. Since the point of suspensions is a node, the eigen frequencies, ω_n, at which the chain resonates occur when:

$$\xi_i = 2\,\omega_n\sqrt{\frac{z_i}{g}}\ , \tag{12}$$

where ξ_i is a zero of $J_o(x)$, n is the number of nodes on the chain, and z_i is the location of the i^{th} node from the top of the chain. Squaring both sides of Equation 11 and taking the difference between adjacent nodes yields:

$$\xi_i^{\,2} - \xi_{i-1}^{\,2} = \frac{4\,\omega_n^{\,2}}{g}(z_i - z_{i-1})\ . \tag{13}$$

A plot of $\xi_i^2 - \xi_{i-1}^2$ versus $z_i - z_{i-1}$ (the internode distances) should yield a straight line with a slope of $\frac{4\,\omega_n^{\,2}}{g}$.

If the initial conditions: $r = 0$ when $z = L$, are put into Equation 11:

$$J_o\left(2\,\omega\sqrt{\frac{L}{g}}\right) = 0\ . \tag{14}$$

Solving for the zero's of the Bessel function gives

$$2\,\omega\sqrt{\frac{L}{g}} = \xi_n\ . \tag{15}$$

Equation 15 relates the zero's of the $J_o(x)$ Bessel function to the frequency with a particular number of nodes, ω_n, and the length of the chain. Equation 15 allows us to predict the frequency knowing only the length of the chain and the number of nodes.

THE EXPERIMENT

For this investigation, we used different lengths of the same chain. Each link was shaped like a three-dimensional figure eight. The plane of the top half of each link was perpendicular to the bottom half. The mass/length, λ, of the chain was 13.05 gm/m.

The chains were held in a chuck fastened to a rotation motor [3] shaft by a single set screw. The set screw was adjusted until the chuck rotated uniformly as observed from different angles. [4] We used a cathetometer to measure the internode distances for the chains shorter than one meter. For the longer chains, we used a 2-meter stick.

To find the nodes, we began at roughly 0 rev/sec, slowly increasing the frequency, being careful not to touch the chain in any way. When we found a stable structure, we turned off the motor and then restarted it. [5] By doing this, each node was created from the same initial conditions. [6]

We used the software statistics package *StatMost* [7] to plot the difference between the squared Bessel function, $J_o(x)$, zeros versus the internode distances. From the slope of this line and using Equation 13, we determined the calculated frequency for this structure.

DISCUSSION

Figure 2 is the plot of the difference between the squared Bessel function, $J_o(x)$, zeros versus the internode distances of a 1.50 meter chain with 5 nodes oscillating at the first occurring or first order stability. The calculated frequency for this first order structure agrees with the measured frequency of the motor to within 2%, a good agreement.

Figure 3, a plot of the difference between the squared Bessel function, $J_o(x)$, zeros versus the internode distances for the second order stability of a 1.5 meter long chain with 4 nodes. The calculated frequency for this case is a factor of 1.4 smaller than the measured frequency of the motor.

Table 1 shows all of our results for different length chains, different numbers of nodes and different orders of stability. For all of the first order stabilities, the calculated frequencies determined from graphs such as shown in Figures 2 and 3 and measured frequencies were within 3% of each other. The first order frequencies are also consistent with those predicted by Equation 15.

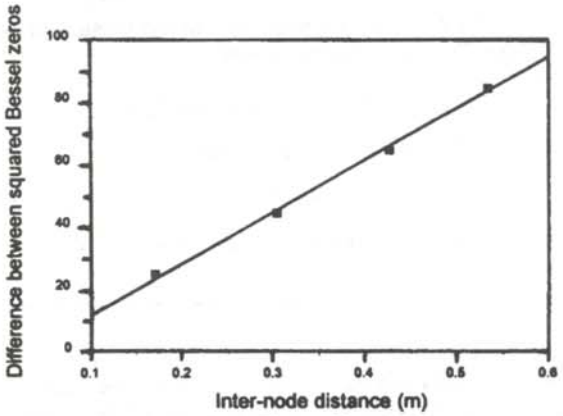

Figure 2

Difference of the squared Bessel function, $J_o(x)$, versus the internode distance for the first order stability of a 1.5 meter chain with 5 nodes.

The measured frequency of the motor for a second stability appears to be roughly 1.5 times greater than the calculated value. The measured frequency for the motor for the third order stability runs is roughly 2.0 times the calculated value. The consistency of these numbers led us to believe that there may be a deeper relationship between the frequency and the characteristics of the chain than is given in Equations 13 and 15.

We suspect that the number of nodes possible is also a function of the length. Longer chains allow for more nodes. This is possibly due to a lower limit for the internode distances. We were not able to get an internode distance of less than 0.12 meters. This lower limit may be the result of the size and mass of the links. For a chain with larger links , such as ours, the lower limit for the internode distance would be relatively high. The same would be true for a heavy chain. The nodes need to be farther apart to have visible antinodes.

Using a strobe light, we discovered that in the first order stability, the chain goes through one complete rotation of the wave for every one rotation of the chuck. We call this the "precession-like motion" of the wave. The individual links also complete one rotation. This motion we call the spin of the links. Using the same strobe frequency, we can "stop" the rotation of the chuck (the precession of the wave) and the links (the spin of the individual links). This motion is similar to that of the moon moving around the earth. The earth represents the z-axis about which the chain rotates. The precession of the chain is represented by the moon moving about the earth. The spin of the chain represents the moon's rotation. Just as the same side of the moon always faces the earth, the same side of each link always faces the z-axis.

At higher order stability, this is not the case. There are two different rotations occurring within the chain at a higher order stability. Each link completes more than one rotation for every precession of the larger wave. Rather than the moon moving about the earth, it is like the earth moving about the sun. The spin frequency of each link at higher order stability is equal to the frequency supplied by the motor. The precession frequency of the chain is the same as for the first order stability. Western's theory is correct only for the precession frequency.

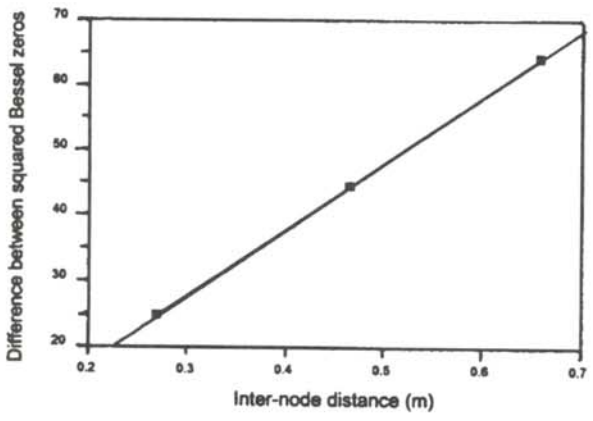

Figure 3
Difference of the squared Bessel function $J_o(x)$ zeros versus the internode distance for second order stability of a 1.5 meter chain with 4 nodes.

Length (nodes)	Order of Stability	Calculated Frequency rad/sec	Motor Frequency rad/sec	Ratio
.50 (3)	1	20.4±0.2	19.0±0.2	0.93
.75 (3)	1	16.5±0.2	16.4±0.2	0.99
	2	17.7±0.7	29.3±0.9	1.66
	3	18.0±1.0	44.2±0.7	2.46
1.00(3)	1	14.3±0.2	14.0±0.2	0.98
	2	14.1±0.1	22.0±0.3	1.56
	3	14.2±0.2	29.3±1.2	2.06
	4	14.2±0.1	36.2±0.2	2.55
1.25(3)	1	12.5±0.3	12.2±0.1	0.98
	2	12.0±0.2	19.5±0.9	1.62
	3	12.4±0.2	24.2±0.6	1.97
1.50(3)	1	11.4±0.2	11.1±0.2	0.97
	2	11.6±0.3	17.4±0.1	1.50
	3	11.3±0.1	21.4±0.2	1.89
2.00(3)	1	9.9±0.1	9.6±0.1	0.97
1.00(4)	1	19.8±0.4	19.2±0.2	0.97
	2	20.5±0.2	30.1±0.1	1.47
1.50(4)	1	15.7±0.3	15.4±0.1	0.98
	2	15.7±0.2	22.2±1.3	1.41
	3	15.9±0.1	27.4±0.9	1.72
2.00(4)	1	13.5±0.1	13.3±0.4	0.99
1.50(5)	1	19.9±0.2	19.5±0.2	0.98
2.00(5)	1	17±0.1	16.7±0.1	0.98

Table 1
Results of the frequency measurements for various length chains with different numbers of nodes and different orders of stability.

ACKNOWLEDGMENTS

The author wishes to thank Wilfred Norris for his interest and guidance; Norm Siems and Ray Pfrogner for their valuable suggestions and assistance; Dan Nelson for his assistance with the theory; and Aaron Blanchard for his thought provoking questions.

REFERENCES

* Current address of author: 120 Wilbur Street, Apartment F4, Newark, DE 19711, Lacy@UDel.edu.

1. A.B. Western, "Demonstration for Observing $J_o(x)$ on a resonant rotating chain.", Am. J. Phys., 28, 1, (Jan 1980), pp. 54-56.
2. This is supported by a plot of the Bessel functions of zero order. A good plot can be found in Abromowitz and Stegun, Handbook of Mathematical Functions, Dover Publications, Inc., New York, (1972).

3. Our rotation motor was manufactured by Cenco, model number 74350. The motor supplying the power was a General electric AC motor, model number 5KH23AAC305, running at 1725 RPM.
4. If the chuck was not centered, it would rotate about a two dimensional space rather than a fixed point.
5. True resonance is self-starting.
6. There was actually a range of stability. We used the first instance of stability within this range because it showed the most defined nodes.
7. StatMost for Windows, DataMost Corporation, 1994.
8. Abromowitz and Stegun, Handbook of Mathematical Functions, Dover Publications, Inc., New York, (1972).
9. Frank Bowman, Introduction to Bessel Functions, Dover Publications, Inc.. New York, (1958).

FACULTY SPONSOR

Professor Wilfred G. Norris
Department of Physics
Juniata College
Huntingdon, PA 16652-2119

NEUTRON SCATTERING: Magnetic Flux Tube

Andrei Teodor Filip * and Dan Adrian Mazilu †
Department of Physics
Alexandru Ioan Cuza University
Iasi, Romania
received May 25, 1996

ABSTRACT

Applying the commonly used partial wave method of the quantum theory of collisions, the asymptotic wave solution of a polarized neutron beam scattered from a flux tube with a constant axial magnetic field are derived. Expressions for the phase shifts and the scattering cross-sections are derived. When the incident neutron beam is polarized perpendicular to the magnetic field direction, the scattering cross-sections of the two opposite spin components exhibited profoundly different features. The significance of this phenomenon and its application to the study of vortex structure in type-II superconductors are discussed.

INTRODUCTION

In previous works : Neutron Scattering: Constant Magnetic Field Band [1] (NSI); Neutron Scattering: Pöschl-Teller Potential [2] (NSII), we discussed the spin-dependent effects in one-dimensional neutron scattering by magnetic fields and the application to the study of the characteristics of the magnetic field. In this paper, we extend our study of neutron scattering by magnetic fields to a three-dimensional case: an infinitely long tube with radius *a* (see Figure 1). The magnetic field ***B*** that does the scattering, confined inside the tube, is constant and pointing along the +*z* direction. There is a strong resemblance between this simple structure and the magnetic flux tube in type-II superconductors. [3]

There is no difference in the fundamental mechanism of superconductivity in type-I and type-II superconductors [4]. In both types, the mechanism is the same and they have similar thermal properties at the superconducting-normal transition in zero magnetic field. But a good type-I superconductor, e.g. Nb, exhibits the so-called Meisner effect, it excludes a magnetic field until superconductivity is destroyed suddenly and completely, and then the field

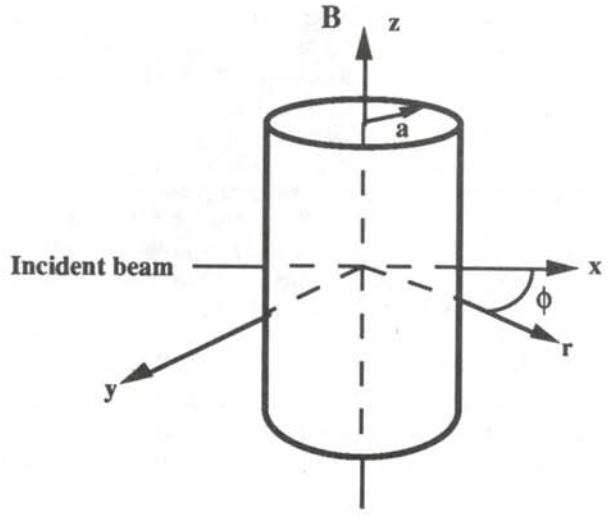

Figure 1
Geometry of the scattering experiment. The flux tube is an infinitely long cylinder of radius a and with axial magnetic field B

When this research was done, Andrei Filip and Dan Mazilu were applied physics majors at the Alexandru Ioan Cuza University of Iasi, Romania. Andrei is a junior and Dan is a senior. In the spring of 1994, they came to the University of Nebraska at Omaha as exchange students. During their stay, they accomplished the first part of this work. After they returned to Romania, Andrei and Dan continued to work on the problem and extended the idea to a three-dimensional case which constitutes the major part of this paper.

At the end of 1995, Dan was selected by his department to visit the Catholic University of Leuven, Belgium where he took courses on magnetic film fabrication before graduation. Dan was accepted at the State University of New York at Buffalo for graduate study. He has recently transferred to Virginia Polytechnical and Sate University in Blacksburg Virginia.

Andrei was chosen to visit the University of Groningen in the Netherlands. He is working with the Quantum Monte Carlo Computation Group. He will stay there for a semester.

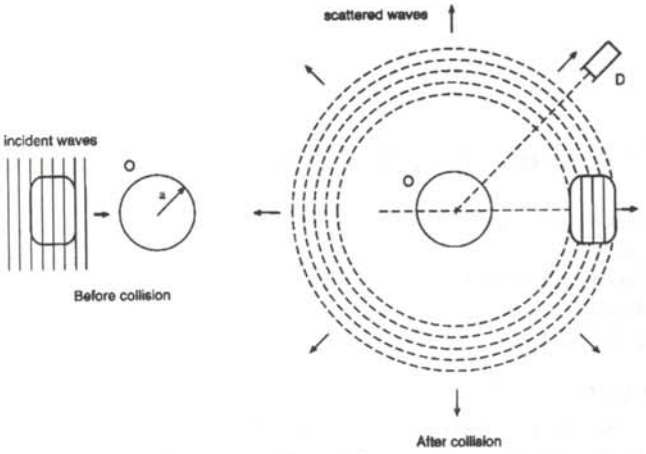

Figure 2
Schematic diagram of the scattering. The neutron beam impinges from the left, strikes the flux tube O and is collected by the detector D.

penetrates completely. However, a good type-II superconductor, e.g. Nb_3Sn, remains electrically superconducting when magnetic fields below a certain critical value are trapped inside. In type-II superconductors, superconductivity persists when the magnetic field approaches 100 kG. Thus, they are considered to have very important technological applications. The trapped magnetic fields arrange themselves into a regular lattice of fluxoids or flux vortices with the shape of a long cylindrical tube. Within each vortex, there is a definite amount of flue, one flux quantum = hc/2e = 2.07x10-7 G cm2. The core region of the fluxoid is essentially in normal phase. The radius of the flux vortex will be of the order of the coherence length, the thickness of the boundary between the normal and superconducting phases [4].

A polarized neutron beam, with magnetic moment pointing either in the $+y$ or $-y$ direction, coming in from the $-x$ direction, should be an excellent probe to scrutinize the interior magnetic field distribution of such a flux vortex.

THEORY

If the flux tube (shown in Figure 1) is infinitely long and the neutron beam impinges perpendicular to the tube axis, we can make full use of the cylindrical symmetry and reduce the three-dimensional scattering problem to a two-dimensional problem (see Figure 2). The incident neutron beam can be expressed as a plane wave:

$$\Psi_k^o(\vec{x}) = \exp[ik\rho\cos(\varphi)] = \sum_{m=-\infty}^{\infty} i^m e^{im\varphi} J_m(k\rho)\,, \quad (1)$$

where $J_m(x)$ is the Bessel function [4] of order m, and k is the wave vector of the incident particle. The scattered wave which lies outside the potential region ($\rho>a$) can be written as

$$\Psi_k^+(\vec{x}) = \frac{1}{2}\sum_{m=-\infty}^{\infty} i^m e^{im\varphi}\,[H_m^{(1)}(k\rho)\,e^{2i\delta_m} + H_m^{(2)}(k\rho)]\,, \quad (2)$$

where δ_m is the phase shift due to the presence of the potential and $H_m^{(1)}(k\rho)$ and $H_m^{(2)}(k\rho)]$ are Hankel functions [4] of the first and second kind respectively:

$$H_m^{(1)}(x) = J_m(x) + i\,N_m(x)$$
$$H_m^{(2)}(x) = J_m(x) - i\,N_m(x)\,, \quad (3)$$

where $N_m(x)$ is the Neumann function (or Bessel function of the second kind) [5] of order m. The two Hankel functions have different behavior at the origin as well as in the asymptotic region. We use both of them when describing the wave function outside the potential region ($\rho>a$). Since the wave function has to be finite at the center of the tube, the wave function inside the potential region ($\rho<a$) can be written as:

$$\Psi_{in}(\vec{x}) = \sum_{m=-\infty}^{\infty} B_m i^m e^{im\varphi} J_m(k'\rho)\,, \quad (4)$$

where k' is the wave vector inside the potential region and B_m is a coefficient which can be obtained by matching the wave functions and their derivatives at the boundary of the tube ($\rho=a$). Matching Equation 2 and Equation 4 at the boundary give the phase shifts as:

$$\tan(\delta_m) = \frac{k'\,J_m'(k'a)\,J_m(ka) - kJ_m(k'a)J_m'(ka)}{k'\,J_m'(k'a)\,N_m(ka) - kJ_m(k'a)N_m'(ka)}\,, \quad (5)$$

where

$$J_m'(x) = \frac{dJ_m(x)}{dx}\,, \quad (6)$$

and

$$N_m'(x) = \frac{dN_m(x)}{dx}\,, \quad (7)$$

The derivatives of the Bessel functions can be evaluated using the recurrence relations for $J_m(x)$ and $N_m(x)$ respectively [5].

From the phase shifts, δ_m, we can determine the total scattering cross-section, σ. The cross-section provides us with the full dynamic and structural information about the potential. The total scattering cross-section for scattering from a long cylinder is [6,7]:

$$\sigma = \frac{4}{k}\sum_{m=-\infty}^{\infty}\sin^2(\delta_m)\,. \quad (8)$$

The scattering cross-section depends explicitly on the incident energy and implicitly on the magnetic field inside the flux tube through the phase shifts δ_m.

If the incoming particle beam is monochromatic in energy, it has kinetic energy:

$$E = \frac{\hbar^2 k^2}{2\mu}\,, \quad (9)$$

where μ is the neutron mass and $\hbar$ is Planck's constant. According to conventional electromagnetic theory, the interaction energy between the magnetic moment of the neutron μ_n and the magnetic field $\boldsymbol{B}$ is given by

$$U = -\boldsymbol{\mu}_n \cdot \boldsymbol{B}\,, \quad (10)$$

where

$$\mu_n = -1.91\frac{e\hbar}{2\mu c} .$$

The negative sign in the neutron's magnetic moment is due to the special characteristic of the neutron, the direction of the magnetic moment is experimentally found to be opposite to that of its spin angular momentum.

Contrary to the classical picture of the magnetic moment, spin has a special "quantum" character. Even though the neutron beam is polarized along the +*y* or -*y* direction, it has two equal and nonvanishing components parallel and antiparallel to the magnetic field ***B*** which points in the +*z* direction. These two components interact differently with the magnetic field. In the one-dimensional case (NSI and NSII), this particular feature profoundly influenced the transmission and reflection coefficients of the polarized neutron beam. We showed that this two-component nature of the neutron's spin and the opposite orientation to the spin states, the energies of the neutrons inside the flux tube are:

$$\frac{\hbar^2 k'^2}{2\mu} = \frac{\hbar^2 k^2}{2\mu} \pm \mu_n B , \qquad (11)$$

where the "+" corresponds to the states with spin "up" and the "-" corresponds to the spin states opposite to the magnetic field. We expect that a similar phenomena will be manifest in two dimensions. The spin up neutrons "see" an attractive potential, just as if they were passing over a potential well, while the spin down neutrons "see" a repulsive potential, as if they were tunneling through a potential barrier. Therefore, the wave vector *k'* inside the flux tube depends on the spin orientations of the incident neutron.

From Equation 10, we can recognize that the wave vector *k* for the spin up neutron is always positive. Thus, the scattering cross-section calculated using Equation 8 with the phase shifts obtained from Equation 5 is real and positive. However, the spin down case is different. When the interaction energy is greater than the kinetic energy, the wave vector k' inside the magnetic field region becomes imaginary. We replace the Bessel function $J_m(x)$ with an imaginary argument in Equation 5 by the modified Bessel function 4:

$$J_n(ix) = i^n I_n(x) . \qquad (12)$$

The expression for the scattering cross-section (Equation 8) is still the same, but the expression for the phase shifts δ_m becomes:

$$\tan(\delta_m) = \frac{k' I_m'(k'a) J_m(ka) - k I_m(k'a) J_m'(ka)}{k' I_m'(k'a) N_m(ka) - k I_m(k'a) N_m'(ka)} , \qquad (13)$$

where

$$k' = \sqrt{\frac{2m}{\hbar^2}\mu_n B - k^2} , \qquad (14)$$

and

$$I_n'(x) = \frac{dI_n(x)}{dx} . \qquad (15)$$

The derivative of $I_n(x)$ can be evaluated using the recurrence relations. [4]

Making use of the properties of the Bessel functions we can prove that in Equations 5 and 13,

$$\delta_m = \delta_{-m} \qquad (16)$$

Hence, the summation in Equation 7 is reduced by half.

Making use of the asymptotic expressions and the recurrence relations of the Bessel functions, we can show that the phase shifts expressed in Equation 13 are real and finite. Thus, the scattering cross-section given by Equation 8 is positive and definite, even when the magnetic energy is greater than the kinetic energy of the neutron.

RESULTS AND DISCUSSION

Using Equation 5 for the kinetic energy, we numerically calculated the scattering phase shifts of a spin parallel neutron beam from the magnetic flux tube with a constant axial magnetic field B and radius a. The scattering cross-section (Equation 8) was then evaluated and plotted as a function of the kinetic energy, E, of the neutron beam. The results are shown in Figures 3 - 5. We varied the size of

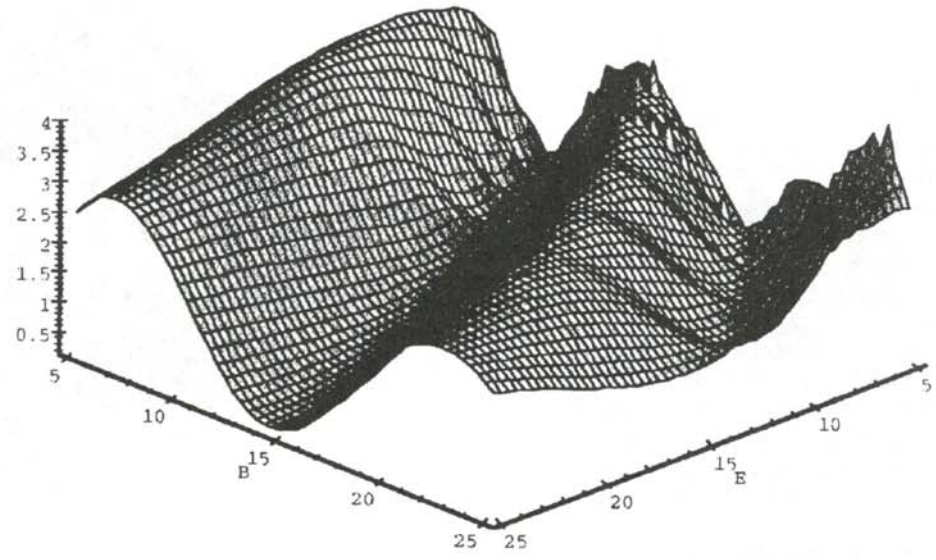

Figure 3

Three dimensional plot of the scattering cross-section σ (x 10-7 m) for parallel spin neutron beam as a function of the kinetic energy E (x 10-26J) and magnetic field B (T). The radius of the tube is 500 Å.

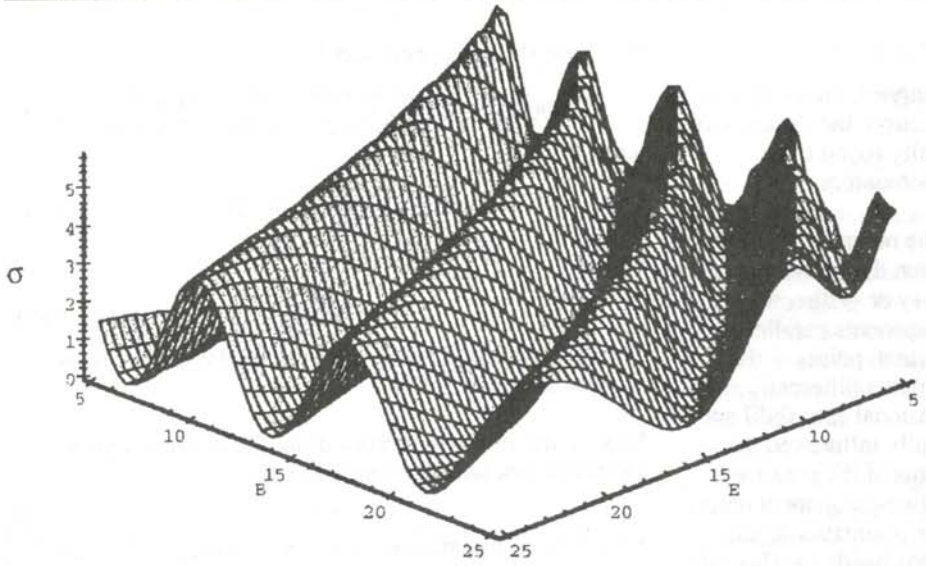

Figure 4

Three dimensional plot of the scattering cross-section σ (x 10-7 m) for parallel spin neutron beam as a function of the kinetic energy E (x 10-26J) and magnetic field B (T). The radius of the tube is 1000 Å.

the radius of the flux tube from 500 Å to 2000 Å to show the structural dependence of the cross-section.

The cross-section oscillates as the magnetic field increases. The number of oscillations increase as the radius increases. This behavior is analogous to that we observed in the tunneling probability of one-dimensional potential wells; the incident wave stays longer in the wider potential.[2]

For the spin antiparallel neutron beam, we used Equations 5 and 13 to calculate the phase shifts; the same set of parameters as used for the spin parallel case we calculated the scattering cross-section. These results are shown in Figures 6 - 8. The cross-section changed abruptly when the kinetic energy, E, crossed from the region where it was greater than the magnetic energy, $\mu_n B$, to the region where it was smaller. This behavior was also noticed in NSI and NSII: when the kinetic energy of the incident neutron beam is lower than the height of the potential barrier, the penetration drops exponentially.

To demonstrate this oscillatory behavior, we chose the range of the kinetic energy to be 5x10-26J and 25x10-26J and the magnetic field to range between and 5T - 25T . In view of the sensitive variations shown in Figures 3 - 8, it is natural to propose using this technique to study the structure and magnetic field distributions of type-II superconductor flux vortices. However, one must realize that the neutron beam kinetic energy is too low and the magnetic field is too strong for a realistic experiment. Unless one can achieve much higher magnetic fields in the laboratory, or discover a neutral particle with a much larger magnetic moment, such an experiment will remain "gedanken".

SUMMARY

We extended the neutron scattering study from one-dimensional potentials to a three dimensional system: an infinitely long tube with a constant axial magnetic field confined inside. Our study concentrates on the spin-dependent effects in the scattering experiments. We analytically found the phase shifts and scattering cross-sections for the two opposite spin components. Numerical calculations showed that the two spin orientations behaved remarkably different within the incident energy and magnetic field ranges we chose. To obtain the phase shift expressions analytically, we restricted our model to a constant magnetic field. It is a

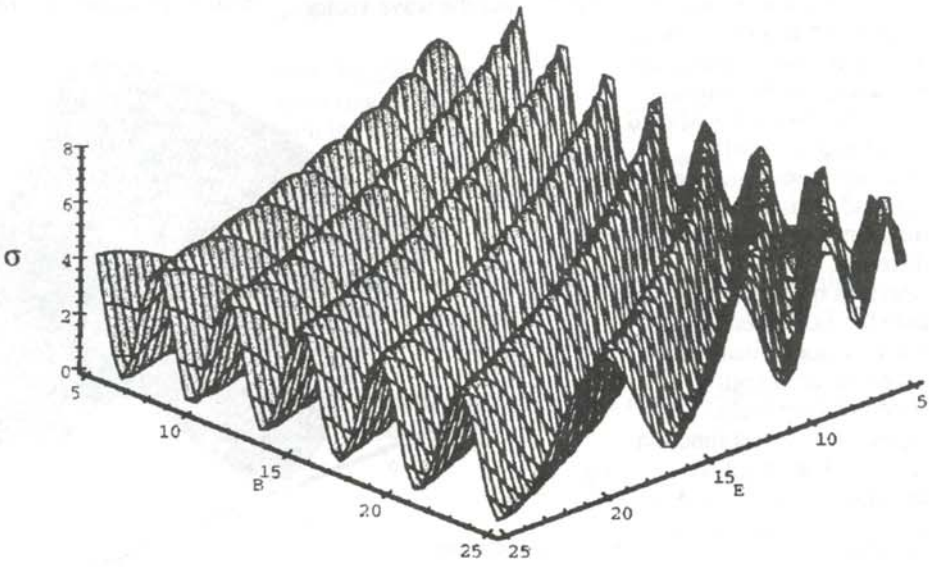

Figure 5

Three dimensional plot of the scattering cross-section σ (x 10-7 m) for parallel spin neutron beam as a function of the kinetic energy E (x 10-26J) and magnetic field B (T). The radius of the tube is 2000 Å.

straight forward task to extend this formalism to a magnetic field distribution with cylindrical symmetry. We plan to study the scattering by more complex field distributions.

ACKNOWLEDGMENTS

We would like to thank Professors Glen Sowell and Steven Dunbar for their guidance on using the MAPLE plotting software package. We also thank Professor Wai-Ning Mei for his invaluable support.

REFERENCES

* Present address of Andrei Teodor Filip: Department of Physics, University of Groningen, Netherlands.

† Present address of Dan Adrian Mazilu: Department of Physics, State University of New York at Buffalo, Amherst, NY 14260.

1. T.D. Burnes II and S.L. Stenberg, The Journal of Undergraduate Research in Physics, 12, 11, (1993).
2. D.A. Mazilu and A.T. Filip, The Journal of Undergraduate Research in Physics, 14, 3, (1995).
3. A.A. Abrikosov, JETP, 5, (1947).
4. C. Kittel, Introduction to Solid State Physics, 5th Ed., John Wiley, New York, (1976).
5. M. Abramowitz and I.A. Stegun, Handbook of Mathematical Functions, Dover, New York, (1972).
6. S.K. Adhikari, American Journal of Physics, 54, 362, (1986).
7. P.J. Cumpson, American Journal of Physics, 58, 659, (1990).

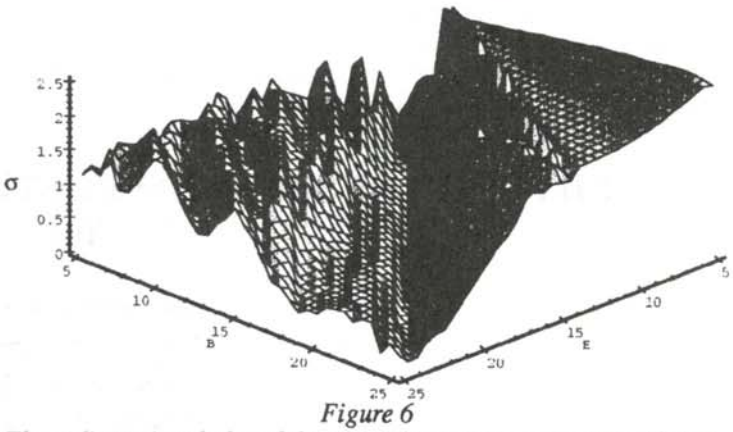

Figure 6

Three dimensional plot of the scattering cross-section σ (x 10-7 m) for antiparallel spin neutron beam as a function of the kinetic energy E (x 10-26J) and magnetic field B (T). The radius of the tube is 500 Å.

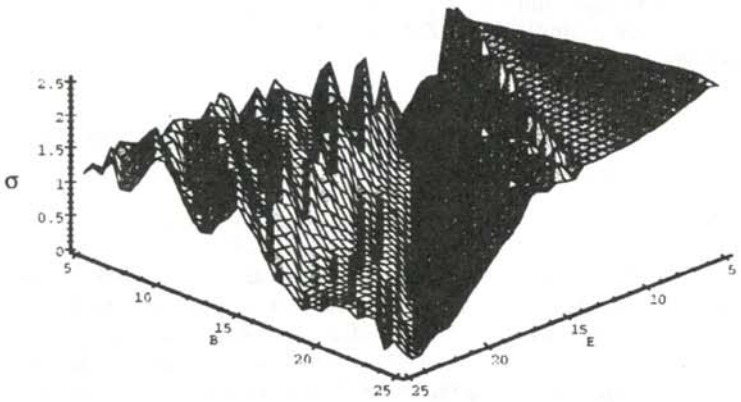

Figure 7

Three dimensional plot of the scattering cross-section σ (x 10-7 m) for antiparallel spin neutron beam as a function of the kinetic energy E (x 10-26J) and magnetic field B (T). The radius of the tube is 1000 Å.

FACULTY SPONSOR

Professor W.N. Mei
Department of Physics
University of Nebraska-Omaha
physmei@cwis.unomaha.edu

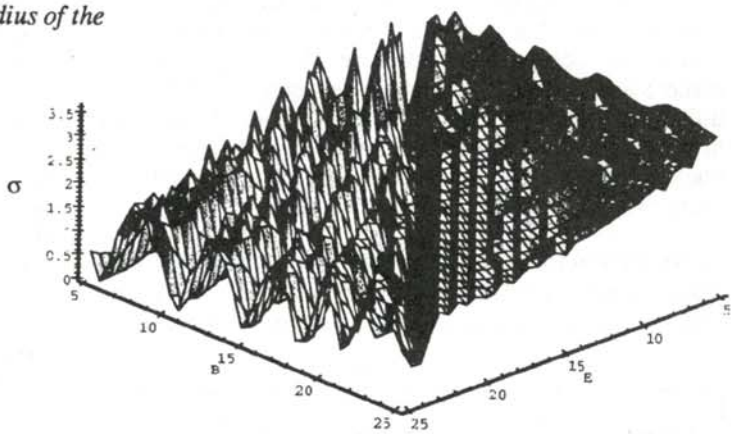

Figure 8

Three dimensional plot of the scattering cross-section σ (x 10-7 m) for antiparallel spin neutron beam as a function of the kinetic energy E (x 10-26J) and magnetic field B (T). The radius of the tube is 2000 Å.

DIFFUSION OF SOLAR ENERGETIC PARTICLES: A Numerical Study

Kenneth B. Baile *
Physics Department
Roanoke College
Salem, VA 24153
received June 20, 1996

ABSTRACT

The Fokker-Planck equation typically is used to model solar energetic particles (SEP) traversing the heliosphere. In this numerical study, a Gaussian distribution function and a linear approximation to it for the initial value functions will be used to model the transport of SEP generated by a solar flare. Both the convection and the diffusion coefficients are assumed to be constants in the Fokker-Planck equation, linear partial differential equations which we solve numerically. The only non-linearity introduced is the initial-value function. It is shown that a simple linearized form of the Gaussian initial functions can give rise to spurious and numerically inherent oscillations..

THE HELIOSPHERE

The inner solar system is described as "permeated by swiftly flowing charged particles emanating from the sun, a continuous torrent of solar wind that often blows in sudden gusts"[1]. In this chaotic atmosphere, solar flare particles are ejected from the Sun in a spiral pattern due to the Sun's rotation. Particles traverse the sun's magnetic fields until reaching an abrupt discontinuity in space, the outer edges of the heliosphere. The heliosphere is a bubble which surrounds and extends past the solar system. At the edge of this bubble exists a barrier in which particles, depending on energy levels, either stop, are reflected back into the solar system, or pass through and enter the interstellar medium [2]. A similar phenomenon occurs when solar energetic particles (SEP) collide with a planet's atmosphere. In 1964 the heliosphere and the diffusion of particles (mostly protons, but also helium and heavier nuclei with energies of few tens of MeV per nucleon) in this turbulent medium was first described using the Fokker-Planck transport equation.

THE FOKKER-PLANCK DIFFUSION EQUATION

The Fokker-Planck Diffusion equation (FPDE) is a typical partial differential equation (PDE). It is parabolic and consists of terms that are first order in time and second order in space:

$$\frac{\partial \omega}{\partial t} = -\frac{\partial}{\partial r}(F\omega) + \frac{\partial}{\partial r}\left[\frac{\partial}{\partial r}(D\omega)\right] \qquad (1)$$

where $\omega(r,t)$ represents the SEP distribution function that is diffusing in time and space, F is a variable describing the convection velocity of ω due to the solar wind, the diffusion coefficient, D, describes ω's diffusion efficiency and r represents the radial distance from the point in which the particles are ejected[2]. The first term in Equation 1, $-\partial/\partial r\,(F\omega)$, is the convection velocity of ω. The second term, $\partial/\partial r\,(\partial D\omega/\partial r)$, represents the diffusion of ω. D and F together represent the chaotic spiral of SEP traversing through the heliosphere; therefore, D and F are generally nonlinear functions of r. For this study, results at $r = 1$ AU, the diameter of the earth's orbit, will be presented.

As with all PDE's, Equation 1 requires the specification of initial and/or boundary conditions to complete the system of mathematical equations. These equations in this paper will be referred to as auxiliary conditions. Analytically, the principle solution is an easy solution for the FPDE. This solution solves the FPDE for a delta function initial distribution. The delta function describes a physical situation created at an infinitesimal time and space (e.g. a solar flare). The idealized nature of the delta function limits the applicability to physical examples. Realistic modeling requires more complicated form of initial functions (e.g. a Gaussian function); however, these more complicated functions applied to the FPDE may not have analytical solutions. The complexity in solving the FPDE

Kenneth B. Baile graduated from Roanoke College in 1995. He is presently employed at the Naval Surface Warfare Center Dahlgren Division. He is currently working on Ship Integration of Unmanned Aerial Vehicles.

forces a search for alternative solution methods, such as numerical solutions, for more realistic applications.

The FPDE is based on two physical laws: Fick's law and the continuity equation. Fick's law is a rule of transport processes that relates the net transport of material across a unit surface to the gradient of the material density in a direction perpendicular to the unit area[3]. For a constant D, Fick's law takes the form:

$$J = -D\frac{\partial \omega}{\partial r}\ , \qquad (2)$$

where J is the flux. The flux is defined as density times velocity. The continuity equation expresses the conservation of what is being diffused (number of particles):

$$\frac{\partial \omega}{\partial t} + \frac{\partial J}{\partial r} = 0\ . \qquad (3)$$

Combining the two equations gives the FPDE without the convection term [3].

$$\frac{\partial \omega}{\partial t} = D\frac{\partial^2 \omega}{\partial r^2}\ . \qquad (4)$$

Adding the convection term to this equations leads to the FPDE, Equation 1.

APPLICATION TO DIFFUSION OF SEP

A random-walk formalism can be used to sadistically describe the chaotic process that SEP undergo as they transverse the heliosphere. SEP traveling the heliosphere will encounter small scale magnetic irregularities forcing the particles to random-walk. This makes SEP diffusion a Markoff process, describable by FPDE [2]. Particles generated by a solar flare created at the surface of the sun will be carried away from the sun by the diverging solar wind. "During the solar cycle, the tilt of the magnetic equatorial plane changes along with rising and falling solar activity. This tilt, combined with the rotation of the sun, creates a spiral geometry...as the solar wind carries the trapped magnetic field outward" [1]. Figure 1 shows a representation of the heliospheric current sheet as seen from 60 AU from the sun, at an inclination angle of 45° with respect to the ecliptic plane. In this chaotic and on the average spiral away from the sun, SEP will encounter small scale magnetic irregularities on the order of 10^5 km to 10^7 km, which cause the SEP to diffuse mostly parallel to the magnetic lines of force rather than perpendicular to them [2].

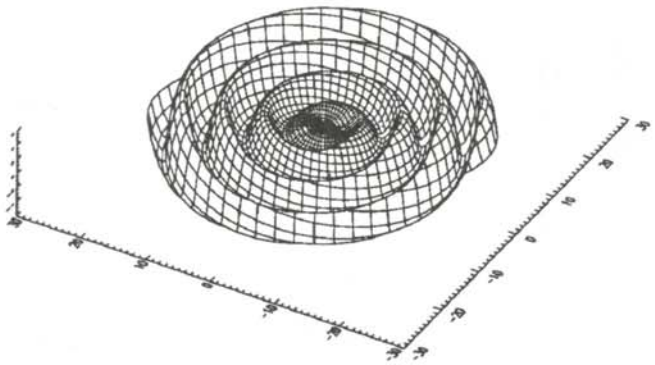

Figure 1
A representation of the heliospheric current sheet as seen from 60 AU from the sun, at an inclination angle of 45° with respect to the ecliptic plane.

The primary diffusing agent of SEP then is the magnetic irregularities carried off by the solar wind. The solar wind convects the SEP at 350 km/sec to 700 km/sec. The typical solar flare particle loses about half of its energy before either, escaping, reflecting, or stopping at the edge of the heliosphere (some 100 AU from the sun). SEP will totally diffuse at 20 AU, beyond the Earth's magnetosphere. These SEP will reach the Earth in 1 or 2 days. The diffusive nature of the outward transport by the solar wind allows the energy intensity of the SEP to peak well beyond the earth's orbit. In general, if SEP encounter a boundary such as the Earth's magnetosphere or the edge of the heliosphere, the SEP will reflect, stop, or "break through" the boundary.

FPDE WITH LINEAR AND NONLINEAR AUXILIARY CONDITIONS

Most physical interactions in general are nonlinear, meaning the interaction has intricately interdependent variables. In this case, an example of non-linearity is SEP traveling through the heliosphere with space dependent diffusion coefficients. The variables that affect the SEP travel through the heliosphere are: the solar wind; the magnetic fields of the planets; and other anomalies which occur in space. Non-linearity is mathematically defined as a function with one or more dependent variables whose variables and derivatives are not raised to a power of one. Non-linearity can also occur in the auxiliary conditions, i.e. initial conditions, or in the derivatives of the dependent variable. An example of non-linearity in the FPDE is when the diffusion coefficient D is a function of space:

$$D = D(r)\ . \qquad (5)$$

In this case, Equation 1, now with nonlinear terms, becomes:

$$\begin{aligned}\frac{\partial \omega}{\partial t} &= -\frac{\partial (F\omega)}{\partial r} + \frac{\partial}{\partial r}\left[\frac{\partial}{\partial r}(D\omega)\right] = \\ &-\frac{\partial (F\omega)}{\partial r} + \frac{\partial}{\partial r}\left[\frac{\partial D}{\partial r}\,\omega(r,t) + \frac{\partial \omega(r,t)}{\partial r}D\right] = \\ &-\frac{\partial (F\omega)}{\partial r} + \frac{\partial^2 D}{\partial r^2}\,\omega(r,t) + 2\frac{\partial D}{\partial r}\frac{\partial \omega(r,t)}{\partial r} + \frac{\partial^2 \omega(r,t)}{\partial r^2}D\ .\end{aligned} \qquad (6)$$

Non-linearity occurs when the partial derivative in Equation 6 is taken, producing more dependent terms. Depending on the complexity of F, Equation 6 may not have an analytical solution; therefore, numerical solutions are used to solve this type of equation.

These types of equations, though more applicable to physical processes, are extremely difficult to solve analytically. One method to reduce the complexity of the

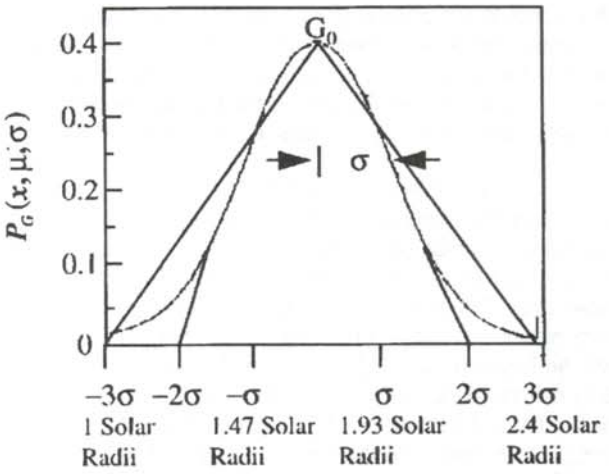

Figure 2
Gaussian probability distribution function and its linear approximation.

equation is to apply a linear approximation to the nonlinear PDE. A simple example of a linear approximation is assuming the diffusion coefficient to be a constant.

$$D = \text{Constant} \ . \tag{7}$$

In this case, Equation 1 becomes linear:

$$\frac{\partial \omega}{\partial t} = -\frac{\partial (F\omega)}{\partial r} + D\frac{\partial^2}{\partial r^2}\omega(r,t) \ . \tag{8}$$

With F and D being constant, and with an initial delta function solution; the solution to Equation 8 is still mathematically complex:

$$\omega(r,t) \ \alpha \ [\omega_1 \omega_2 \omega_3 \{\omega_4 + \omega_5\} + \omega_6 \omega_7] \ . \tag{9}$$

where ω_1 is a power function in t, ω_2 is an exponential function of r, ω_3 is an exponential function of t, ω_4 and ω_5 are Gaussian in r and t, ω_6 is an exponential in r and ω_7 is an incomplete gamma function where the lower limit depends on both r and t. [5] The addition of any nonlinear terms in the FPDE (e.g. initial conditions not described by the delta function) will make the equation analytically intractable.

MODELING SEP GENERATED FROM SOLAR FLARES

The FPDE will be used to model SEP generated by a solar flare. In this numerical study, the initial probability of locating a SEP's position during the solar flare will be represented by a nonlinear Gaussian distribution function (e.g. non-auxiliary condition). In addition, a linear approximation of the Gaussian distribution will be used as an auxiliary condition for comparison. A numerical solution will be used to solve the FPDE for the two different auxiliary conditions, based on the so-called "method of lines" [4].

Several assumptions were made in this model to idealize the phenomenon for our purposes:

1- Solar wind's speed is a constant (F = 400km/s).
2- Diffusion coefficient is a constant (D = 3 x 10^{21} cm2/s).
3- SEP are assumed to convect radially away from the sun rather than in a three dimensional spiral pattern (i.e. one dimensional in space).
4- The SEP was diffused to 1 AU where it encountered a barrier (magnetosphere) and reflect back into the heliosphere.

The Gaussian distribution and the linearized auxiliary conditions used to model the initial position of the SEP have the form:

$$\omega(r,t=0) = G_o \exp\left[-\frac{(r-\bar{r})^2}{2\sigma^2}\right] \tag{10}$$

and

$$\omega(r,t=0) = .57r + 1 \quad 1 \le r < 1.7$$
$$\omega(r,t=0) = -.57r + 1 \quad 1.7 \le r < 2.7 \ . \tag{11}$$

In Figure 2, the linear approximation to the Gaussian is drawn over the Gaussian distribution function. The Gaussian and the linear approximation have a peak value of G_0 = 1.7 solar radii. The Gaussian has a standard deviation of .28 solar radii. Therefore, the most probable initial position of the SEP will occur between 1.47 solar radii and 1.93 solar radii. Both auxiliary conditions originate around one solar radii and have the same area under the curve up to 12%. At G_o, the two lines were overlapped in Figure 2, showing the linear function has a

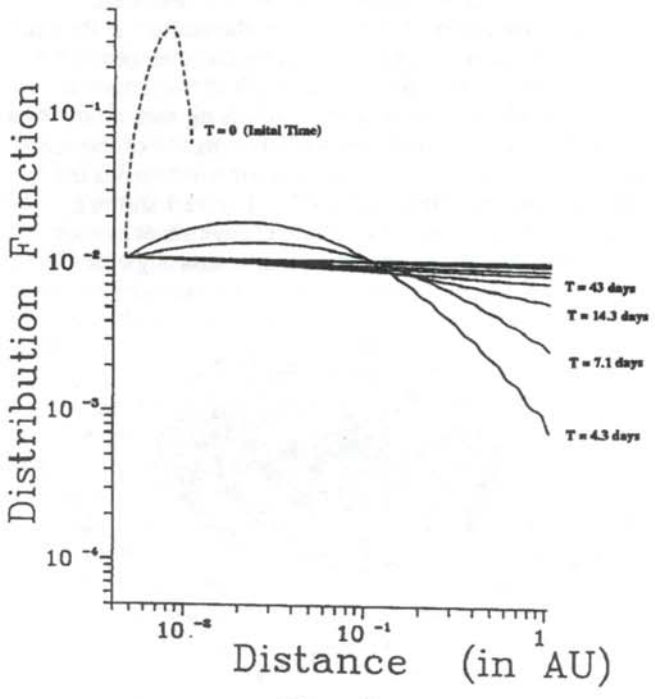

Figure 3
Numerical solution for the diffusion of SEP in position and time using the linear approximation to the Gaussian initial conditions.

discontinuity in the first derivative, whereas the Gaussian function is continuous.

RESULTS AND DISCUSSION

Numerical techniques reduce complex partial differential equations with no known analytical solutions to solvable algebraic equations. An example of this would be reducing a PDE to a set of algebraic equations. In our case, Equation 1 is first reduced to a set of ordinary differential equations (functions of r only) at a particular t. These finite difference ODE's are now algebraic equations, which can be solved using tri-diagonal methods. The solution at different times are then integrated using the Runge-Kutta method. [7]

Figures 3 and 4 show the results of our numerical calculations: how the distribution of SEP changes with time due to diffusion. Figure 4 uses the nonlinear Gaussian initial conditions, while Figure 4 uses the linear approximation to the Gaussian function. Comparing the results from the two numerical solutions of the Fokker-Planck equation, the linearization of the Gaussian distribution appears in the solution for only small time scales. In Figure 3, "oscillations" occur at time values of T= 4.3, 7.1, 14.3, and 43 days the linear approximation; however, in Figure 4, these "oscillations" do not occur. The discontinuity in the derivatives of the linear approximation of the Gaussian function can cause the oscillations for small time scales in the diffusion of SEP generated by a solar flare. For large time scales, however, the initial condition of modeling the solar flare does not matter because the SEP are totally diffused.

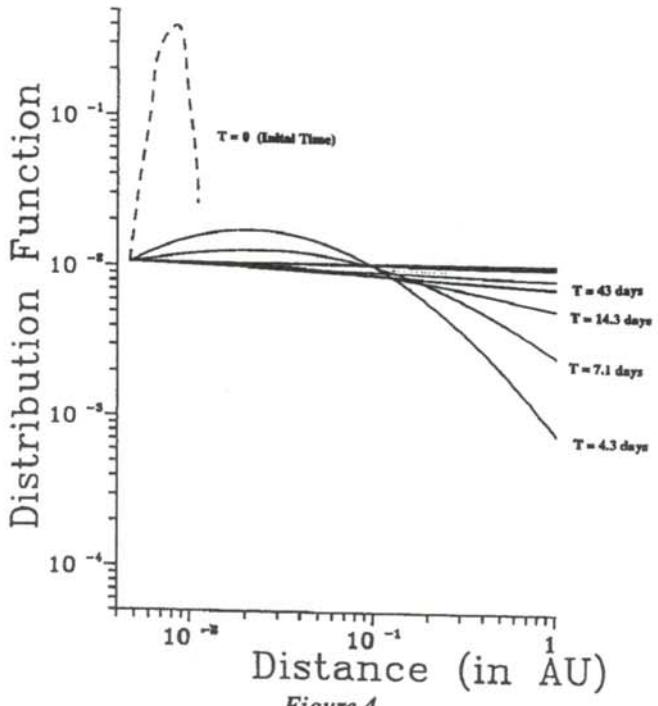

Figure 4
Numerical solutions for the diffusion of SEP as a function of distance and time. This set of solutions was for Gaussian initial conditions.

When one is interested in transient solutions at small time scales, linearizing an initial Gaussian distribution function and diffusing it in time and space may cause spurious oscillations that are inherently numerical in nature. Similar spurious inherently numerical behaviors have been seen in numerical solutions of PDE's with discontinuous boundary conditions [8].

ACKNOWLEDGMENTS

This work would not have been possible without the help and support of my advisor Professor A. F. Barghouty.

REFERENCES

* Current address of the author: 9854 Dominion Forest Circle, Fredericksburg, VA 22408, KBBaile@nswc.navy.mil.

1. J. R. Jokipii and Frank McDonald, "Quest for the Limits of the Heliosphere", Scientific American, Vol. 272, No. 4, April, 1995. pp.59-63.
2. E. N. Parker, "The Passage of Energetic Charged Particles Through the Interplanetary Space." Planet Space Sci., Vol 13, (1965), pp 9-49.
3. Elliott Montroll and Bruce West, On an Enriched Collection of Stochastic Processes, Physical Dynamics, Inc. Elsevier Science Publishers B.V. (1979).
4. W.E. Schiesser, The Numerical Method of Lines: Integration of Partial Differential Equations, Academic Press: San Diego, (1991).
5. J.R. Jokipii and B.Thomas, "Effects of Drift on the Transport of Cosmic Rays IV, Modulation by a Wavy Interplanetary Current Sheet", Astrophysical Journal, 243, (1981), pp. 115-1122.
6. E. Wong, "The Construction of a Class of Stationary Markoff Process", Proc. Sympo. Applied Math, 16, (1964), p. 246.
7. J. Stoer and R. Bulirsch, Introduction to Analysis, Springer-Verlag, New York.
8. R.A. Nouy and H.T. Davis, "A Comparison of Synthetic Boundary Conditions for Continuous Flow Systems", Chem. Eng. Sci, 46, p. 50.

FACULTY SPONSOR

Dr. A.F. Barghouty
Physics Department
Roanoke College
Salem, VA 24153
BARGHOUTY@aleph.Roanoke.Edu

ADIABATIC POPULATION TRANSFER IN A THREE LEVEL ATOM

J.V. Ruffo *
Department of Physics and Astronomy
University of Rochester
Rochester, NY 14627
received July 15, 1996

ABSTRACT

We have studied analytically and by computer simulation the laser-induced transfer of an electron from one atomic level to another. The transfer is stimulated by a Raman-type process. Two laser fields, usually called "pump" and "Stokes", are responsible for the transfer. The population transfer resulting from the so-called "counter-intuitive" pulse sequencing scheme, in which the Stokes laser pulse arrives before the pump pulse, is studied. We call attention to some advantageous features of this type of sequencing. We show that the transfer can be successfully characterized by an "adiabatic" approximation.

INTRODUCTION

In many applications, it is desirable to transfer an electron in an atom from one energy level to another. This may be a direct transfer, involving only two atomic levels, or may involve some intermediate levels that the electron must pass through before coming to its final state. The model we deal with here incorporates one such intermediate level, so we consider three atomic levels in all. Our model allows for the possible loss of the electron, via collisional excitation, spontaneous emission or some other process. We define a parameter, γ, in units of frequency, which is proportional to this loss rate. The model is illustrated in Figure 1.

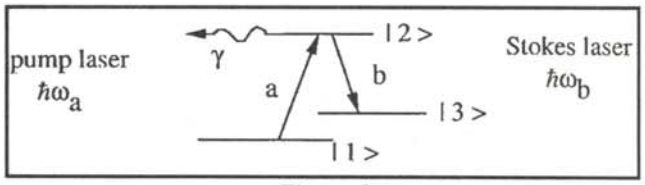

Figure 1
Atomic transitions and corresponding lasers. The arrow labeled γ indicates the possible loss of the electron from the three-level system via level |2>.

In carrying out the transfer from state |1> to state |3> as shown in Figure 1, it seem most natural first to attempt to excite the electron from its initial state |1> to the intermediate state |2> using a laser pulse (labeled 'pump' in Figure 1) and then to de-excite the electron into the final atomic state |3> via another laser pulse ('Stokes' in Figure 1). However, in the work, we consider the situation where one pulse precedes the other in the manner shown in Figure 2.

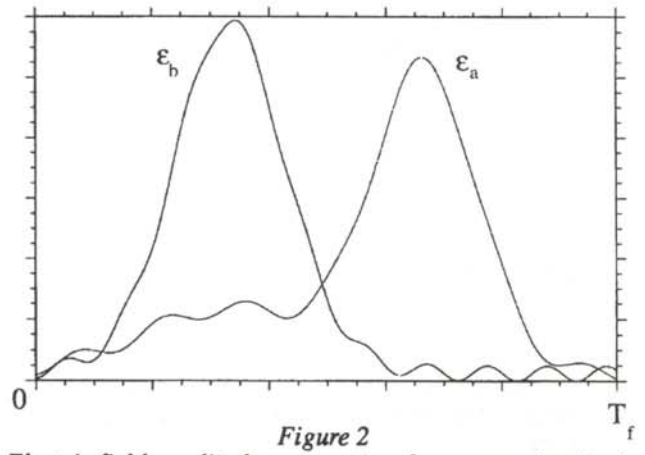

Figure 2
Electric field amplitudes versus time for counter-intuitively sequenced pulses. The Stokes laser, labeled "b" precedes the pump laser, labeled 'a'.

Jim graduated from the University of Rochester in 1996 with a B. Sc. in physics and a B.A. in mathematics. He was president of the Rochester Sigma Pi Sigma. His thesis was awarded an honorable mention in the university's Stoddard Prize competition. Jim's research began in collaboration with W. Grana during June-August, 1995, while participating in a summer research program sponsored by the NSF at the university. In December, he accepted a position with SVG Lithography in Connecticut. For relaxation he plays his guitar, and enjoys sake boarding. If the snow ever comes to New England, he is looking forward to snow boarding as well.

In this case, where the Stokes pulse precedes the pump pulse, we say that the pulses are 'counter-intuitively' sequenced [1]. In particular, we are concerned with the resulting efficiency of transfer from state |1> to state |3>. We present results that confirm that it is possible to obtain nearly 100% efficiency using this counter-intuitive approach [1].

MATHEMATICAL PRELIMINARIES

We take the Hamiltonian for the system to be:

$$\bar{H} = \bar{H}_a + \bar{V} \ , \qquad (1)$$

where $\bar{H}_a$ is the atomic Hamiltonian and $\bar{V}$ is the laser-atom interaction energy. Using the dipole approximation:

$$\bar{V} = -\,\bar{d}\cdot\vec{E}(t) \ , \qquad (2)$$

where $\bar{d} = e\,\bar{r}$ is the dipole moment operator and $\vec{E}(t)$ is the combined electric field vector of the two lasers, which is treated classically and not as an operator.

We begin by assuming that the frequencies of the lasers are equal to the frequencies associated with the atomic transitions. We thus only consider the interaction of the atom with the electric fields of the two laser pulses, which we take to be quasi-monochromatic and linearly polarized:

$$\vec{E}(t) = \bar{x}\left[\varepsilon_a(t)\left(e^{-i\omega_a t} + e^{i\omega_a t}\right) + \varepsilon_b(t)\left(e^{-i\omega_b t} + e^{i\omega_b t}\right)\right]. \qquad (3)$$

Furthermore, we use a three-level approximation, that is, we assume an atomic wave function of the form:

$$|\Psi(\bar{r},t)> = c_1(t)\,|1> + c_2(t)\,|2> + c_3(t)\,|3> \ . \qquad (4)$$

After inserting the three-level wave functions into Schrödinger's equation:

$$i\hbar\,|\dot{\Psi}(\bar{r},t)> = \bar{H}\,|\Psi(\bar{r},t)> \ , \qquad (5)$$

and operating on the left with <il, i = 1,2,3, we obtain three coupled differential equations for the $c_i(t)$'s, one for each value of i:

$$\begin{aligned} i\hbar\,\dot{c}_1 &= E_1 c_1 - \left(\vec{d}_a\cdot\vec{E}(t)\right)c_2 \\ i\hbar\,\dot{c}_2 &= -\left(\vec{d}_a\cdot\vec{E}(t)\right)c_1 + E_2 c_2 - \left(\vec{d}_b\cdot\vec{E}(t)\right)c_3 \\ i\hbar\,\dot{c}_3 &= E_3 c_3 - \left(\vec{d}_b\cdot\vec{E}(t)\right)c_2 \ , \end{aligned} \qquad (6)$$

where

$$\begin{aligned} H_a|i> &= E_i\,|i> \\ \vec{d}_a &= <1|e\,\bar{r}|2> = <2|e\,\bar{r}|1> \\ \vec{d}_b &= <3|e\,\bar{r}|2> = <2|e\,\bar{r}|3> \ . \end{aligned} \qquad (7)$$

The probability amplitudes must be normalized:

$$|c_1|^2 + |c_2|^2 + |c_3|^2 = 1 \ . \qquad (8)$$

A rotating wave approximation (RWA) can be used to simplify Equations 6. We begin by defining new variables [2]:

$$\begin{aligned} a_1(t) &= c_1(t)\,e^{-iE_1 t/\hbar} \\ a_2(t) &= c_2(t)\,e^{-i\left(E_1+\hbar\omega_a\right)t/\hbar} \\ a_2(t) &= c_2(t)\,e^{-i\left(E_1+\hbar\left(\omega_a-\omega_b\right)\right)t/\hbar} \ . \end{aligned} \qquad (9)$$

These new amplitudes remain normalized:

$$|a_1|^2 + |a_2|^2 + |a_3|^2 \equiv |c_1|^2 + |c_2|^2 + |c_3|^2 = 1 \ . \qquad (10)$$

The RWA neglects rapidly oscillating terms and replaces very slowly oscillating terms by 1. After applying the RWA and substituting Equations 9 into Equation 6, we obtain a set of differential equations for the $a_i(t)$'s, which can be written in matrix form as:

$$i\frac{d}{dt}\begin{bmatrix} a_1 \\ a_2 \\ a_3 \end{bmatrix} = -\frac{1}{2}\begin{bmatrix} 0 & \Omega_a & 0 \\ \Omega_a & 2i\gamma & \Omega_b \\ 0 & \Omega_b & 0 \end{bmatrix}\begin{bmatrix} a_1 \\ a_2 \\ a_3 \end{bmatrix}. \qquad (11)$$

Here, we have defined

$$\Omega_a = \frac{2\left(\vec{d}_a\cdot\bar{x}\right)\varepsilon_a}{\hbar}, \quad \Omega_b = \frac{2\left(\vec{d}_b\cdot\bar{x}\right)\varepsilon_b}{\hbar}, \qquad (12)$$

which are called the Rabi frequencies of the interactions. We inserted the parameter γ into the Hamiltonian matrix in Equations 11. As a parameter associated exclusively with the |2> state, γ can be shown to have a damping effect, allowing the population in state |2> to decay at a rate proportional to γ.

Momentarily regarding the Hamiltonian matrix as constant at a specific time, T, its eigenvalues and eigenvectors can be found by solving the eigenvalue equation:

$$-\frac{1}{2}\begin{bmatrix} 0 & \Omega_a & 0 \\ \Omega_a & 2i\gamma & \Omega_b \\ 0 & \Omega_b & 0 \end{bmatrix}\begin{bmatrix} a_1 \\ a_2 \\ a_3 \end{bmatrix} = \lambda\begin{bmatrix} a_1 \\ a_2 \\ a_3 \end{bmatrix}. \qquad (13)$$

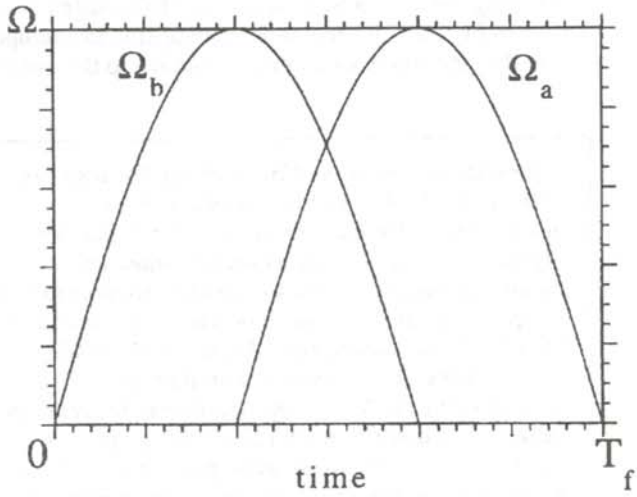

Figure 3

Time dependence of Ω_a and Ω_b. Note that Ω represents the peak value of both Ω_a and Ω_b.

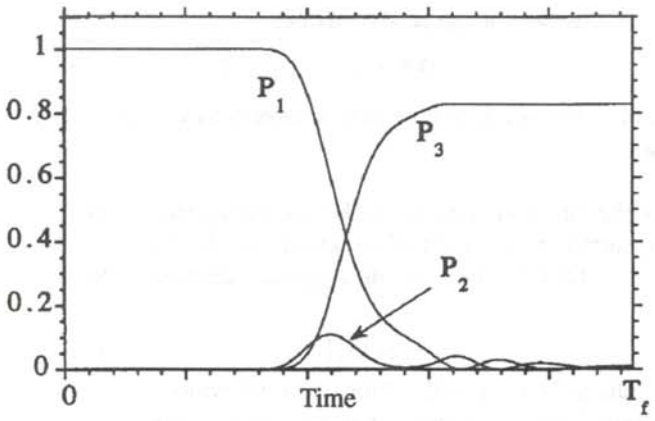

Figure 4
Probabilities for each of the levels |1>, |2> and |3> versus time; $T_f = \frac{3\pi}{2\Omega}$, $\Omega = 10\gamma$.

Solving Equation 13, we obtain:

$$|\varphi_\pm\rangle = \frac{1}{\sqrt{K^2 + 4|\lambda_\pm|^2}} \begin{bmatrix} \Omega_a \\ 2\lambda_\pm \\ \Omega_b \end{bmatrix}, \quad |\varphi_0\rangle = \begin{bmatrix} \Omega_b \\ 0 \\ -\Omega_a \end{bmatrix}$$

$$\lambda_\pm = \frac{-i\gamma}{2} \pm \frac{1}{2}\sqrt{K^2 - \gamma^2}\ , \quad \lambda_0 = 0 \qquad (14)$$

$$K(T) \equiv \sqrt{\Omega_a^2(T) + \Omega_b^2(T)}\ .$$

It should be emphasized at this point that T is merely a parameter and should be regarded as different from the true 'dynamical' time, which we have called t. For this reason, the variation of Ω_a and Ω_b as a function of T is called a 'parametric' variation of the Hamiltonian.

For convenience, and to limit the number of free parameters, we model the time dependence of Ω_a and Ω_b by a half-cycle sine wave

$$\Omega(t) = \Omega \sin(\alpha t) \qquad (15)$$

which displaces the time origins. Since Ω_a and Ω_b are directly proportional to the electric field amplitudes, if we make Ω_a and Ω_b functions of time in Equation 11, it has the effect of making ε_a and ε_b functions of time as well as indicated in Figure 3.

When the electric field amplitudes are time-dependent (leading to a time dependent Hamiltonian matrix), Equation 11 cannot be solved analytically. Thus, we use a Runge-Kutta method [3,4] to integrate Equation 11 numerically. From the numerical solutions for the $a_i(t)$'s, we can calculate the probabilities:

$$P_i(t) = |a_i(t)|^2 \qquad (16)$$

for each level. Some typical results for the three probabilities are shown in Figure 4.

NUMERICAL RESULTS

For convenience, we measure the Rabi frequencies of Equation 12 in units of γ and time in units of $1/\gamma$. Since the pulse shapes are fixed by Equation 15, there remain two parameters which can be manipulated: the peak strength, Ω, of the pulses and the final time, at which the second pulse is turned off, labeled T_f in Figure 3.

Figures 5a and 5b each show the resulting transfer to |3> for a particular α (or equivalently, T_f) and several values of the peak intensity Ω. Apparently, the efficiency of transfer increases quasi-monotonically as one strengthens the pulses. Also, comparing Figures 5a and 5b, it seems that one can also obtain higher efficiency by lengthening the pulses (i.e. making α smaller). Roughly speaking, one can 'get away with' weaker lasers by lengthening the pulses. This could present useful advantages in experiments.

THE ADIABATIC PRINCIPLE

The adiabatic principle states that if a system is initially in the jth eigenstate of the Hamiltonian at some initial time, then it will be found in the jth eigenstate of the Hamiltonian at some later time, even if the Hamiltonian is time-dependent, provided that the rate of change due to the parametric variation of the Hamiltonian (i.e. how quickly Ω_a and Ω_b are varied) is sufficiently small compared with the rate of change due to the 'natural dynamics' of the system [5]. When we interpret T as the real time, we are

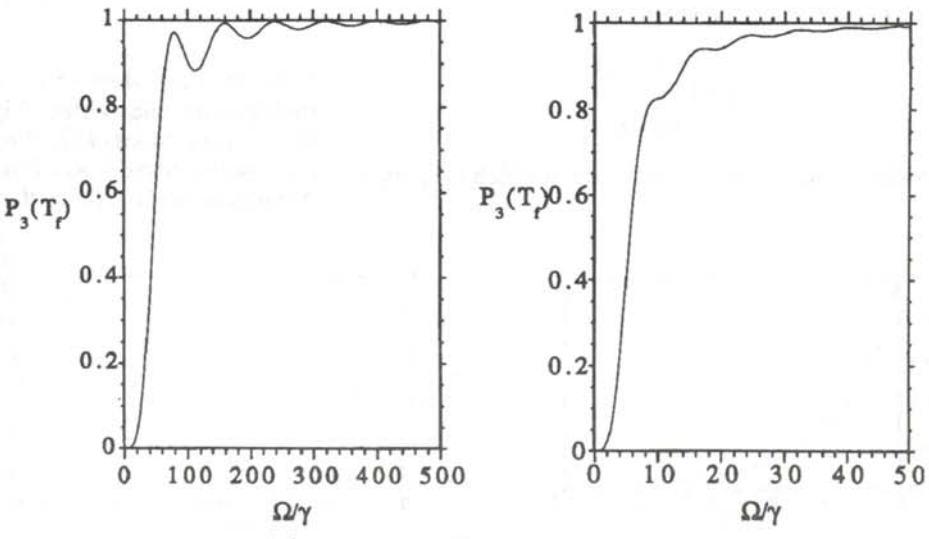

Figure 5
Final probability for |3> (labeled $P_3(T_f)$ versus Ω/γ for a fixed pulse length (represented by α). Nearly perfect transfer can be achieved for sufficiently strong fields (large Ω). (a) $\alpha = 10\gamma$, (b) $\alpha = \gamma$

making a departure from the exact solutions, but we expect this "adiabatic approximation" to be nearly correct if the parametric variation is slow. Now, we will show how to apply this adiabatic principle to counter-intuitive excitation.

Taking the Hamiltonian matrix at a specific time T, we have found the eigenvalues and eigenvectors in Equation 14. The $|\varphi_0>$ eigenstate of Equation 14 is of special interest, because of its properties when Ω_a and Ω_b vary as a function of T in the manner described by Equation 15 and Figure 3:

$$|\varphi_0> = |1> \quad \text{at } T = 0$$
$$|\varphi_0> = |3> \quad \text{at } T = T_f \ . \tag{17}$$

We see that $|\varphi_0>$ corresponds to the true initial state $|1>$ at the beginning and to the desired final state, $|3>$ at the end. Thus, if the atom remains in this eigenstate throughout the entire process, the electron will be found in the $|3>$ state with certainty at T_f. We thus wish to ensure that the system remains in $|\varphi_0>$ after the initial time.

In each of the two temporal regions in which one of the lasers is off ($t < T_f/3$ and $t > 2T_f/3$ in Figure 3), the effect of the remaining laser on the final population in $|3>$ can be neglected. Thus, we can ignore these two regions and focus on the central regtion ($T_f/3 \le t \le 2T_f/3$) where both Ω's are nonzero. In this region, we have (after shifting the time origin to the position formerly called $T_f/3$):

$$\Omega_a = \Omega \sin(\alpha t)$$
$$\Omega_b = \Omega \cos(\alpha t) \tag{18}$$

Note that with this choice, we conveniently have $K(T) = \Omega = constant$, and the normalized $|\varphi_0>$ eigenstate can now be parameterized simply by α:

$$|\varphi_0> = \begin{bmatrix} \cos(\alpha t) \\ 0 \\ \sin(\alpha t) \end{bmatrix} . \tag{19}$$

α provides a measure of the time scale in which the pulses vary. In this case, it can be shown that:

$$\alpha = \frac{\pi}{2T_f} \ . \tag{20}$$

Small α corresponds to long pulses, large α to shorter pulses.

Since the rate of change due to the 'natural dynamics' of the system is controlled by the eigenvalues, $\lambda_\pm$, the condition for the validity of our adiabatic approximation is:

$$\alpha << |\lambda_\pm| \tag{21}$$

using the definitions in Equation 18. Furthermore, recalling Equation 14 and noting that $|\lambda_\pm|$ will have different values depending on the relationship between Ω and γ, the right side of Equation 21 can be simplified:

$$\alpha << \frac{\Omega}{2}, \ \text{if } \Omega \ge \gamma$$
$$\alpha << \frac{\Omega^2}{2\gamma}, \ \text{if } \Omega < \gamma \ . \tag{22}$$

The first result in Equation 22 is arrived at trivially while the second result is derived by expanding the term under the square root in Equation 14. These inequalities identify the adiabatic region for us.

Figures 6a and 6b represent numerically obtained results relevant to both the situation where $\Omega < \gamma$ and to the case where $\Omega = \gamma$. The adiabatic approximation applies to both of these situations in much the same manner. To realize some arbitrary degree of efficiency, the adiabatic condition must be satisfied to the same degree in each case. To achieve an efficiency of about 80% (i.e., $P_3(T_f) = 0.8$), α must be approximately an order of magnitude less than $|\lambda_\pm|$

$$\alpha < \frac{|\lambda_\pm|}{10} \ . \tag{23}$$

In the situation where $\Omega > \gamma$, we obtain results that are slightly more unexpected. Figure 7 shows several results for different values of Ω, plotted against α/Ω, illustrating the resulting transfer as a function of the relative value of α compared to Ω. Notice that for any value of α, the final population in $|3>$ approaches a limiting value as Ω increases, This limiting value of $P_3(T_f)$ remains above 0.8 for $\alpha = |\lambda_\pm|$, in contrast to Equation 23. Evidently, in this region, the condition defined by Equation 22 need not be satisfied in the same of Equation 23 to achieve efficient transfer.

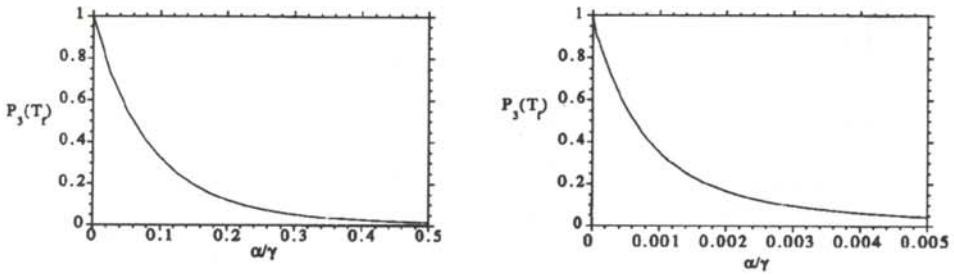

(a) (b)

Figure 6
Final probability for $|3>$ versus α for fixed pulse strength. (a) $\Omega = \gamma$, (b) $\Omega = 0.1\gamma$. Note that longer pulses are represented by decreasing α.

SUMMARY

Our results provide a generalization of known two-level atom results [5]. The use of two

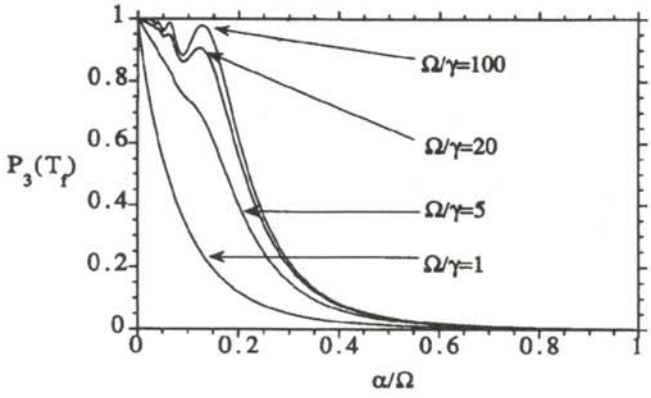

Figure 7
$P_3(T_f)$ versus α/Ω for several fixed values of Ω. Note that $\alpha = |\lambda_{\pm}|$ when $\alpha/\Omega = 0.5$.

laser pulses provides the opportunity to study the effect of pulse sequencing, which is not possible in a two-level, one-laser case.

We have shown that the counter-intuitive approach has several useful features. By solving Equations 11 by numerical integration, we found that for a wide range of values of the parameters (loss and peak laser strength), nearly 100% population transfer is possible. Also, by invoking an adiabatic principle and thus obtaining Equation 21, we were able to identify a controllable parameter (α or equivalently T_f) on which the final population in |3> depends quasi-monotonically. Numerical results confirm this prediction. However, in the case where $\Omega > \gamma$, we show that it is not always necessary for Equation 21 to be satisfied in the sense of Equation 22. Nevertheless, all the results confirm that the adiabatic condition presented is sufficient for efficient transfer.

ACKNOWLEDGMENTS

The work presented in this paper was begun in a collaboration with W. Grana during June-August, 1995. It was supported by the Research Experience for Undergraduates program of the National Science Foundation at the University of Rochester and by NSF Grant number PHY-9408733. The author would like to thank Prof. J.H. Eberly and Dr. C.K. Law for their advice and support.

REFERENCES

* Current Address of the author: 94 Washington St., Apt. 21, Norwalk, CT 06854, RUFFOJ@svg.com

1. An early proposal concerning 'counter-intuitive' pulse ordering can be found in J. Oreg, F.T. Hioe and J.H. Eberly, Phys. Rev A., 29, (1984) p. 690. A previous study with close connections to ours was reported by C.E. Carroll and F.T. Hioe, Phys. Rev. A, 42, (1990), p. 1522, particularly in section V and VI.
2. For an introduction to few-level laser-atom interactions, including the definition of the dipole Hamiltonian, the rotating wave approximation, etc. see J.H. Eberly and P.W. Milonni, *Encyclopedia of Physical Science and Technology*, edited by R.A. Meyers, Academic Press, 1987, Vol 11, pp. 474-477.
3. J.A. Jacquez, *A First Course in Computing and Numerical Methods*, Addison-Wesley, (1970).
4. S. Yakowitz and F. Szidarovszky, *An Introduction to Numerical Computations*, Macmillan, (1989).
5. R. Maruyama, "The Transition Between Adiabatic and Nonadiabatic Dynamic Behavior in a Quantum System", Journal of Undergraduate Research in Physics, 13, 2, (1995), pp. 56-59.

FACULTY SPONSOR

Dr. J.H. Eberly
Andrew Carnegie Professor of Physics
Department of Physics and Astronomy
University of Rochester
Rochester, NY 14527

POST USE BOOK REVIEW

COLLEGE PHYSICS, 4th Ed. by Raymond A. Serway and Jerry S. Faughn
Harcourt Brace, New York, 1995
PHYSICS, 3rd Ed. by John. D. Cutnell and Kenneth W. Johnson
John Wiley and Sons, Inc. New York, 1995

Reviewed by:
Hilary Davis *
Guilford College, Greensboro, NC 27410

College Physics, by Raymond A. Serway and Jerry S. Faughn, is intended for students who are not physics majors and whose avocations are biology/health related. It is intended to be introductory and, in that sense, should be easy to understand, interesting and well-integrated with other disciplines such as medicine and biology. Serway and Faughn do present sections on the integration of biology and physics throughout the text and meet this criteria quite adequately. I was impressed by the discussion of the mass spectrometer in chapter 19 and would suggest that this kind of approach be followed to a further extent. They also provide useful tables on the covers and a quite sufficient table of contents, appendices and index.

The actual discussion of physics concepts, however, is somewhat dry and uninspiring. An good introductory physics text is enlightening and interesting at the same time; perhaps Serway and Faughn might want to consider adopting a more enlightening dialogue when writing further introductory physics texts. They do, however, partly compensate for this deficiency by providing intriguing biography boxes on the scientists involved in the concepts about which they write. However, as a common practice with many textbook writers, there is an obvious shortcoming in providing information about female scientists whose research has been discussed in the book. Beyond the obvious, such as Madame Curie, the writers of most textbooks could improve their efforts by including more biographies of women physicists/researchers whose work is relevant to the scope of the textbooks.

When discussing a concept, Serway and Faughn provide fairly adequate diagrams and pictures. However, they might consider investing more effort in describing the diagrams in more detail in future editions of the text. This text does present at the end of each chapter sufficient summaries reviewing all the equations mentioned in the chapter, but not enough review on the concepts discussed in the chapters. Furthermore, this text does not provide adequate discussion covering physics concepts.

In contrast, John D. Cutnell and Kenneth W. Johnson's *Physics*, 3rd edition, does provide many opportunities to obtain a grasp of physics concepts because they make an effort to express physical ideas in explicit guides or models in each chapter. This is quite useful to the student in the sense that it helps them to learn how to think through a problem before attempting to solve for a numerical value.

Both texts provide decent example problems at the end of each section in the chapters and also provide many problems to work at the end of each chapter with varying difficulty and complexity and incorporating many concepts or applications. Unfortunately, the improper use of significant digits in Serway and Faughn's example problems and in the answers to the odd numbered problems is disappointing considering that one of the first things discussed in the text is the importance of using significant digits. In fact, the answers to some of the odd-numbered problems have been found to be incorrect.

Serway and Faughn do not present an adequate text for an introductory physics course. Cutnell and Johnson's introductory text, however, is much more suited for the purpose of an introductory physics course. It seems to meet all the standards of a good physics text with enlightening descriptions of physics topics and concepts, useful and exciting diagrams and pictures, good integration of physical concepts at the end of each chapter, a satisfactory table of contents, a fine index, very useful tables on the covers, a user's guide, plenty of problems at various levels of difficulty, special topics sections relating the way physics is involved in other disciplines, and a useful set of appendices.

* Current address of the author: 5604 Weslo Willow Circle, Apartment 312, Greensboro, NC 27409

Hilary Davis is a recent graduate of Guilford College with a B.Sc. degree in Biology. She is currently working in the chemistry industry and has applied to graduate school in ethnobiology. In her spare time she is an amateur potter and avidly studies traditional and medicinal uses of plants.

PREPARING A MANUSCRIPT FOR PUBLICATION

Rexford E. Adelberger, Editor

Perhaps the most important thing for you to keep in mind when you write a manuscript which you intend to submit for publication to the Journal of Undergraduate Research in Physics is that the audience that will be reading the paper is junior or senior physics majors. They are knowledgeable about physics, but unlike you, they have not spent as much time trying to understand the specific work which is being reported in your paper. They also can read English well and expect the paper to be written by a colleague, not a robot or an 'all-knowing' computer. There is a big difference between the comments you write in the margin of your lab notebook or what you might write in a technical brief and what you should present in a paper for publication in a scientific journal.

There is a significant difference between a Journal article and keeping a journal. Your laboratory data book should be the journal of what you did. It contains all the data, what you did (even if it was an attempt that turned out to be wrong), as well as comments as to what you were thinking at that time. The Journal article is an discussion of how you would do the research without excursions along blind alleys and hours spent collecting data that were not consistent. The reader should not necessarily be able to completely reproduce the work from the Journal article, but the reader should be able to understand the physics and techniques of what was done.

How a person uses Journal articles to find out about new ideas in physics is often done in the following way. A computerized search using key words in abstracts is done to see what work has been done in the area of interest. If the key words found in the abstract seem to be about the question of interest, the body of the paper is tracked down and read. If the reader wants to find out the finer details of how to reproduce the experiment or the derivation of some equation, the author is contacted for a personal in-depth conversation about the more subtle details.

The general style of writing that should be followed when preparing a manuscript for publication in the Journal is different from what you would submit to your English literature professor as a critique of some other work. The narrative of the paper is intended to do three things: 1) to present the background necessary for the reader to appreciate and understand the physics being reported in the paper; 2) discuss the details of what you did and the implications of your work; 3) lead the reader through the work in such a way that they must come to the same concluding points that you did. When finished with your paper, the reader should not have to go back and try to decide for themselves what you did. Your narrative should lead them through your work in an unambiguous manner, telling them what to see and understand in what you did. The interpretation of the data or calculations should be done by the writer, not the reader. The interpretation of your results is the most important part of the paper.

You should take care to make sure that the material is presented in a concise logical way. You should make sure that your sentences do not have too many dependent clauses. Overly complicated sentences make the logic of an argument difficult to follow. You should choose a paragraph structure that focuses the attention of the reader on the development of the ideas.

A format which often achieves these aims is suggested below:

ABSTRACT : An abstract is a self contained paragraph that concisely explains what you did and presents any interesting results you found. The abstract is often published separately from the body of the paper, so you cannot assume that the reader of the abstract also has a copy of the rest of the paper. You cannot refer to figures or data that are presented in the body of the paper. Abstracts are used in computerized literature searches, so all key words that describe the paper should be included in it.

INTRODUCTION: This is the section that sets the background for the important part of the paper. It is not just an abbreviated review of what you are going to discuss in detail later. This section of the narrative should present the necessary theoretical and experimental background such that a knowledgeable colleague, who might not be expert in the field, will be able to understand the data presentation and discussion. If you are going to use a particular theoretical model to extract some formation from your data, this model should be discussed in the introduction.

Where appropriate, factual information should be referenced using end-notes. When presenting background information, you can guide the reader to a detailed description of a particular item with the statement such as: *"A more detailed discussion of laminar flow can be found elsewhere [1]"*. If you know where there is a good discussion of some item, you don't have to repeat it, just guide the reader to the reference.

How one proceeds from this point depends upon whether the paper is about a theoretical study or is a report on an experiment. The first is a suggested format for papers about experimental investigations and the second one that describes a theoretical piece of research.

Experimental Investigations

THE EXPERIMENT: This section guides the reader through the techniques and apparatus used to generate the data. Schematic diagrams of equipment and circuits are often easier to understand than prose descriptions. A statement such as *"A diagram of the circuit used to measure the stopping potential is shown in Figure 6"* is better than a long elegant set of words. It is not necessary to describe in words what is shown in a diagram unless you feel that there is a very special part which should be pointed out to the reader. If special experimental techniques were developed as part of this work, they should be discussed here. You should separate the discussion of the equipment used to measure something from your results. This section should not include data presentations or discussions of error analysis.

DATA PRESENTATION AND INTERPRETATION OF RESULTS: This is the most important section of the paper. The data (a plural noun) are the truths of your work. This section should lead the reader through the data and how errors were measured or assigned. The numerical data values are presented in tables and figures, each with its own caption, e.g.. *"The results of the conductivity measurements are shown in Table 3"*. It is difficult to follow narratives where the numerical results are included as part of the narrative. Raw, unanalyzed data should not be presented in the paper. All figures and tables should be referred to by their number. Any figure or table that is not discussed in the narrative should be eliminated. Items which are not discussed have no place in a paper.

A Theoretical Study

THE MODEL: This part should consist of a theoretical development of the constructs used to model the physical system

The Journal of Undergraduate Research in Physics

The Journal of Undergraduate Research in Physics is the journal of Sigma Pi Sigma and the Society of Physics Students. It is produced by the Physics Department of Guilford College, Greensboro NC 27410. Inquiries about the journal should be sent to the editorial office.

The Journal of Undergraduate Research in Physics ISSN 0731-3764

Editorial Office -
The Journal of Undergraduate Research in Physics
Physics Department
Guilford College
Greensboro, NC 27410
910-316-2279 (voice)
910-316-2951 (FAX)

Editor -
Dr. Rexford E. Adelberger
Professor of Physics
Physics Department
Guilford College
Greensboro, NC 27410
ADELBERGERRE@RASCAL.GUILFORD.EDU

The Society of Physics Students

National Office -
Dr. Dwight Neuenschwander, Director
Ms. Sonja Lopez, SPS Supervisor
Society of Physics Students
American Institute of Physics
1 Physics Ellipse
College Park, MD 20740
301-209-3007
E-Mail - SPS@AIP.ORG
http://www.aip.org/education/SPS/SPS.htm

President of the Society -
Dr. Robert Fenstermacher
Department of Physics
Drew University

President of Sigma Pi Sigma -
Dr. Jean Krisch
Department of Physics
University of Michigan, Ann Arbor

- EDITORIAL BOARD -